Monitoring of a Sequencing Batch Reactor System with Aerobic Granular Sludge for Textile Wastewater Treatment

Kateřina Staňková

Thesis to obtain the Master of Science Degree in

Biological Engineering

Supervisor: Doctor Nídia Dana Mariano Lourenço de Almeida

Co-Supervisor: Professor Helena Maria Rodrigues Vasconcelos Pinheiro

Examination Committee

Chairperson: Professor Jorge Humberto Gomes Leitão

Supervisor: Doctor Nídia Dana Mariano Lourenço de Almeida

Members of the Committee: Professor João Pedro Martins de Almeida Lopes

January 2016

ACKNOWLEDGMENTS

I would like to thank Prof. Dr. Helena Maria Rodrigues Vasconcelos Pinheiro and Prof. Ing. Jan Páca DrSc. for giving me the opportunity to do this work in Portugal as Erasmus student. It was a great experience for me, I am thankful for that.

Thank to Dr. Nídia Dana Mariano Lourenço de Almeida and Prof. Dr. Helena Maria Rodrigues Vasconcelos Pinheiro for reviewing, correcting and assistance me not only with my English. Thank you very much.

To Rita, thank you for everything, your support and patience were for me more important, than I can say.

Obrigada!

ABSTRACT

The following master thesis was divided into two parts. First part was focused on off-line monitoring of three different sequencing batch reactors (SBRs) with aerobic granular sludge for dye-laden textile wastewater treatment: SBR1 with static feeding with silver nanoparticle (Ag-NP) addition, SBR2 as SBR1 Ag-NPs-free control and SBR3 with different feeding regime - plug-flow. The second part was focused on the development of principal component analysis (PCA) and partial least squared (PLS) models. Off-line monitoring was performed by chemical oxygen demand analysis (COD), measurement of total suspended solids (TSS) and volatile suspended solids (VSS) and UV-Vis spectroscopy. These analyses served to assess the efficiency of textile wastewater treatment of each SBR. SBR1 and SBR2 showed very similar results, suggesting that Ag-NP addition did not hamper dye or COD removal in this study. SBR3 exhibited lower dye removal than the first two reactors, suggesting that the plug-flow feeding strategy is not as effective as the static feeding for color removal. PCA and PLS models were developed using mean-centered UV-Vis spectra of wastewater samples containing suspended Ag-NPs. These models were satisfactory for monitoring wastewater containing Ag-NPs.

Keywords: aerobic granular sludge, sequencing batch reactor, silver nanoparticles, PCA, PLS

CONTENT

LIST OF TABLES

LIST OF FIGURES

LIST OF ABBREVIATIONS

Ag-NPs – silver nanoparticles
AGS – activated granular sludge
AR 14 – Azo dye Acid red 14
CAS – conventional activated sludge
dPAO – denitrifying phosphate accumulating organisms
COD – chemical oxygen demand
FAS – ferrous ammonium sulfate solution
HPLC – high-performance liquid chromatography
MO - microorganisms
ORL – organic loading rate
PC – principal component
PCA – principal component analysis
PLS – partial least squares
PVP – polyvinylpyrrolidon
SBR – sequencing batch reactor
TSS – total suspended solids
UV-Vis spectroscopy – Ultraviolet visible spectroscopy
VSS – volatile suspended solids
WF – whole feed
WWTP – wastewater treatment plant

1. INTRODUCTION

The discharge of textile wastewaters containing dyes into the environment is a major problem in the present time. The increasing demand for textile industry products increases the amount of dyes discharged into the environment and there is an effort to control and reduce these amounts. Also, engineered nanoparticles (ENPs) are now present in many textile industry wastewaters and their fate in subsequent treatments is still unknown. The use of aerobic granular sludge (AGS) for wastewater treatment is an emerging, promising technology, which could be applied also for dye removal. The work described in this thesis falls within this scope.

The main goal of this work was to contribute to assess the effect of ENP in the treatment of dye-containing effluents using AGS. It was based on the operation of three bioreactors with AGS with dye removal ability. The first was operated on a mixed fill regime, with a fixed concentration of silver nanoparticles (Ag-NP) in the feed. The second was identical to the first, without Ag-NP in the feed, serving as an Ag-NP-free control. The third featured a plug-flow fill regime, instead of mixed, without Ag-NP in the feed. Each individual reactor was seeded with activated sludge from a full-scale wastewater treatment plant and granulation was subsequently induced.

Off-line monitoring of these bioreactors was another goal of the work. This monitoring consisted of COD analysis, measurements of total suspended solids (TSS) and volatile suspended solids (VSS) and UV-Vis spectroscopy. This monitoring served to evaluate the effectiveness of the treatment and the biomass load in the reactors.

A third goal of the thesis work was to use PCA analysis and PLS model development from measured UV-Vis spectra to identify and quantify Ag-NP, dye and other components of the bioreactors' feed on mixtures prepared in milli-Q water.

2. LITERATURE REVIEW

2.1 Textile wastewaters

Textile wastewater treatment is of major importance for the human society around the world. This is caused by a great demand for textile commodities, driving the growth of textile industry and the discharge of wastewaters associated with it. The release of colored synthetic compounds into the natural environment is considered the main problem. This is not only because of the pollution in the form of color, but it is also related with the fact that many dyes and their breakdown products in wastewaters are toxic and dangerous to human life. Dyes which are not removed in the treatment of these wastewaters are very stable and may remain in the environment for a long time. On the other hand, another significant problem is the large consumption of drinking water, leading to shortages especially in countries with a lack of potable water resources. This has caused increased efforts in the domain of wastewater recycling (dos Santos et al., 2007). Textile industries are a major target for this, due to the large consumption of water in wet textile processing.

2.2 Dye removal in textile wastewater treatment

The most significant class of dyes in textile processing is the azo dyes. There are many different chemical, physical and biological methods to eliminate dyes from textile wastewaters. Physical-chemical dye removal methods, such as coagulation-flocculation, chemical oxidation and membrane filtration, are usually more expensive than biological treatment, which is among the cheapest options. The biodegradation of azo dyes using bacterial cells proceeds in two steps. The first part is the reaction to cleave the dye's azo linkages (N=N), when the electrons from an electron donor are passed to the N=N bonds, which leads to the formation of aromatic amines. These are generally colorless, though potentially more dangerous for human health than the original azo dye. This step of the biodegradation is performed under anaerobic conditions. The second step is the mineralization of the resulting aromatic amines, which is carried out under aerobic conditions and leads to the removal of the chemical oxygen demand (COD) load associated to the dye. The researches have been carried out with anaerobic granular sludge bioreactors, however in most cases they do not achieve full removal of the dyes. So color removal and full mineralization of the dyes is best achieved through the combination of anaerobic and aerobic conditions. In Fig. 1, this procedure is shown schematically (Muda et al., 2010; van der Zee and Villaverde, 2005).

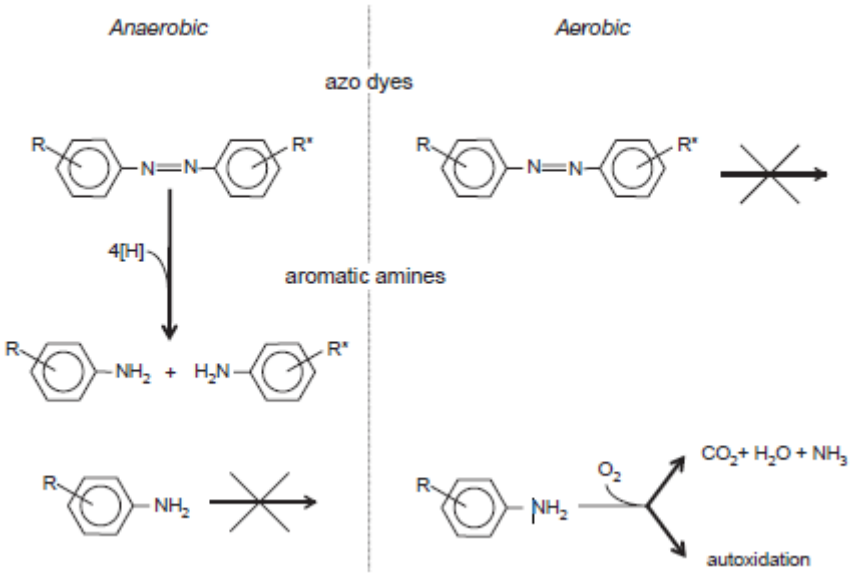

Figure 1– The fate of azo dyes and aromatic amines during anaerobic-aerobic biological treatment (van der Zee and Villaverde, 2005).

Since a combination of anaerobic and aerobic conditions is likely the best option for full azo dye biodegradation, an anaerobic-aerobic sequencing batch reactor (SBR) with activated sludge is one of the promising options (van der Zee and Villaverde, 2005).

2.3 Aerobic granular sludge sequencing batch reactors

The activated sludge process is currently the most used method in biological wastewater treatment. This technique uses mostly flocculent biomass, but recent developments combine it with other biomass forms, such as biofilms and granular sludge. The flocculent sludge is not an entirely suitable treatment method because of problems with sludge settleability, causing biomass washout in secondary clarifiers. Other concerns are the costs of this wastewater treatment option, present and future developments in effluent quality demands, land availability, nuisance aspects (smells, noise) and energy consumption. The use of aerobic granular sludge bioreactors may be the solution to at least some of these concerns (deKreuk et al., 2007, Quan et al., 2015).

Aerobic sludge granulation is the process of conversion of microbial activated sludge aggregates from the floc to the granular morphology, achieved under specific conditions in a sequencing batch reactor. Aerobic granular sludge can be generated with different substrates including glucose, acetate, ethanol, phenol and other synthetic or real wastewater components. The morphological structure of aerobic granular sludge, providing high particle size and density, ensures the main advantages of this wastewater treatment method when compared to the classical activated sludge process. These are a compact design enabled by fast settling and low settled sludge volume, also easing the retention of biomass inside the reactor. It was demonstrated that when the feeding takes place in anaerobic

conditions, it may lead to more stable granules when compared to an aerobic feeding strategy. This type of feeding subject the biomass to alternating feast-famine conditions, which can favor granule stability if biomass activity at its core is maintained. Aerobic granules may be generated across a wide range of organic loading rates from 2.5 to 15 kg COD m^{-3} d^{-1}. Accordingly, AGS presents a promising route in the development of new, compact, and high-rate biological wastewater treatment systems, treating higher wastewater loading rates when compared with conventional activated sludge systems (Isanta et al., 2012; Li et al., 2008; Rocktäschel et al., 2015; Wan and Sperandio, 2009).

In aerobic granular sludge, the co-existence of aerobic and anoxic-anaerobic layers inside the granules has been observed (Winkler et al., 2013). Aerobic (nitrifying) microorganisms can develop at the outer layer of the granules, with easy access to molecular oxygen, where they coexist with the heterotrophs that are the mostly responsible for COD removal. Anaerobic microorganisms (denitrifying phosphate accumulating organisms - dPAO) can accumulate at the inner core and facultative anaerobic microorganisms, such as denitrifiers, PAO and glycogen-accumulating organisms (GAO) can occupy the anoxic and inner aerobic layers in the granule, because of their capability to live under anaerobic and aerobic conditions (Muda et al., 2010; Pronk et al., 2015). In Fig. 2, structural and functional differences between the microbial populations inside aerobic granules and conventional activated sludge flocs are shown.

In this context, the mechanism of biodegradation of azo dyes, as shown in Fig. 1, would possibly be favored by the coexistence of anaerobic and aerobic layers in AGS. Moreover, the high biomass retention times which are achievable in AGS could allow the development of slow-growing organisms (Winkler et al., 2013), enhancing the mineralization potential for the aromatic amines resulting from azo dye bioreduction.

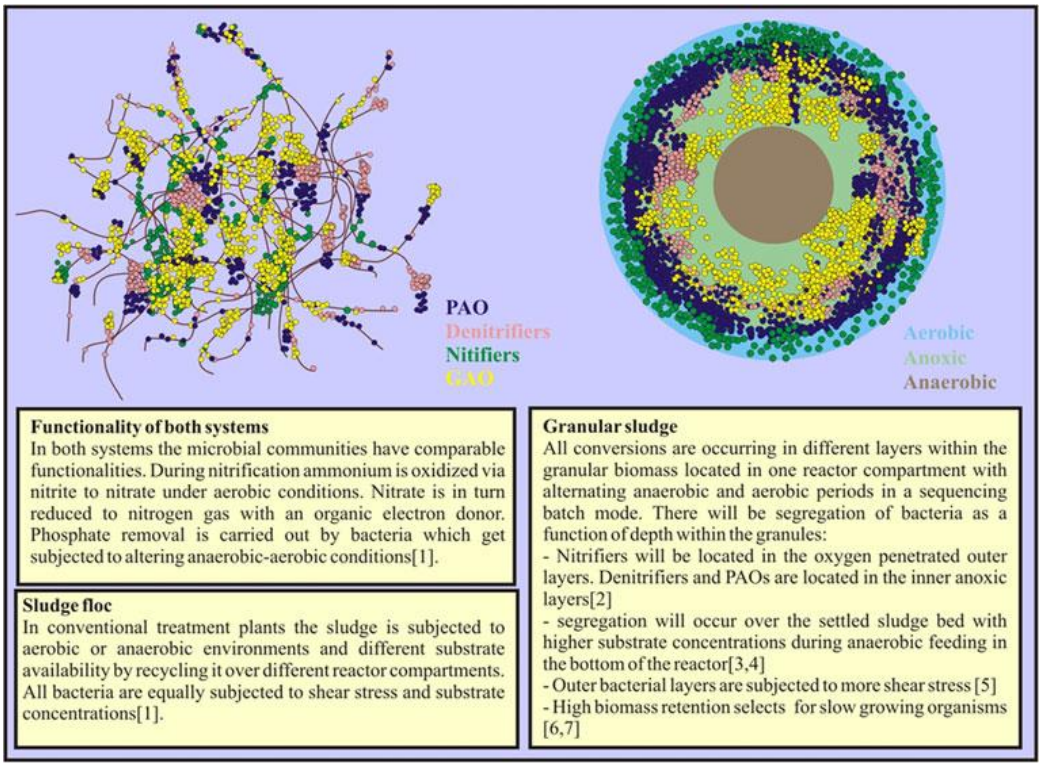

Figure 2 – Comparison of the distribution of microbial community types in aerobic granular sludge and conventional sludge flocs (Winkler et al., 2013).

2.4 Silver nanoparticles

Silver nanoparticles (Ag-NPs), one of the most widely used among ENPs, have often been used in common consumer products, because of their antimicrobial and antiviral properties. They can be found in industrial products, such as antimicrobial Ag-coatings, in hospitals as disinfectants, in other consumer goods, such as mobile phones, clothes, and fridges, and also in the food industry and in drinking water treatment (Kittler et al., 2010). However this increase in nanotechnology applications implies the release of Ag-NPs into the environment, in industrial and domestic waste streams. Their release in wastewaters may be a problem to the treatment systems, because of the toxic effect of Ag-NPs on microorganisms, leading to a decrease in the efficiency of contaminant removal in biological treatment processes (Sheng and Liu, 2011).

It is generally known that dissolved silver ions are much more dangerous for a wide variety of microorganisms than silver nanoparticles. For instance, the lethal silver concentration for human mesenchymal stem cells is three times lower for silver ions than for silver nanoparticles. Accordingly, the rate and degree of silver nanoparticle dissolution has been found to play a major role. They both depend on the chemical species involved, as well as the particle size, surface functionalization and degree of crystallization. The temperature and the nature of the medium in which the particles are immersed are also critical conditions. The degree dissolution also depends on the storage time of the NP suspension. The toxicity of an Ag-NP suspension was found to strongly increase with this time, for which the release of ions was responsible, leading to a 20-fold lower lethal concentration after a period of 6 months later. Partly oxidized nanoparticles are also more toxic than those freshly prepared (Choi

et al., 2008; Kittler et al., 2010). The antimicrobial effect of Ag-NPs is due to the disruption cell membranes, the binding with intracellular proteins and DNA and the release of Ag^+ ions. The latter impedes DNA replication by attacking the thiol groups in the involved enzymes, leading to cell death. This process is promoted by the small size and high surface/volume ratio of silver nanoparticles.

Earlier studies have shown that Ag-NPs could affect both the heterotrophic and autotrophic populations in biological wastewater treatment reactors (Sheng and Liu, 2011). According to the research by Choi et al. (2008), it is especially important to strictly regulate the load of silver nanoparticles coming into wastewater treatment bioreactors, because of the environmentally sensitive nitrifying microorganisms (autotrophic). This research showed that, on the basis of a short-term batch respirometric assay, the inhibition of nitrifying bacteria reached 86 ± 3 % (freshly prepared Ag-NPs) and 42 ± 7 % (Ag^+ ions) for an Ag concentration of 1 mg L^{-1}. The effect of Ag-NPs on heterotrophic growth was also examined. It was found that the inhibition of *Escherichia coli* growth attained 55 ± 8 % (freshly prepared Ag-NPs) and 100 % (Ag^+ ions) at an Ag level of 0.5 mg L^{-1} and no growth was observed at a level of 1 mg L^{-1}. Thus, freshly prepared Ag-NPs revealed higher inhibition potential towards autotrophic microorganisms, but Ag^+ ions were more toxic for the tested heterotrophs.

The structure and morphology of the microbial community is also important for the evaluation of the effect of Ag-NPs, because the different communities respond differently due to varying physico-chemical and microbial properties. Biofilms revealed a stronger tolerance to Ag-NPs than planktonic bacteria. Aerobic granular sludge may be considered as a particular type of biofilm with a more complex and three-dimensional microbial structure. Quan et al. studied the response of AGS to the long-term presence of Ag-NPs in an SBR. AGS was found to tolerate well the presence of Ag-NPs (at Ag levels of 5 and 50 mg L^{-1}), preserving stable microbial activities during the first 35 days of the test. After this period, AGS was found to be inhibited in its oxygen and ammonia respiration rates and denitrification rate. Nevertheless, significant variations in sludge properties were not observed, which preserved large granule size and good settling capability. Thus, Ag-NPs did not cause acute toxicity, but their chronic toxicity effect is a matter of concern (Quan et al., 2015).

2.5 UV-VIS spectroscopy

Ultraviolet-visible (UV-Vis) spectroscopy belongs to compact, relatively low-cost, powerful, fast and simple methods for analysis. This method describes the interaction between samples and radiation in the 200-780 nm wavelength range by measuring absorption areas related to electron transitions between orbitals, which include higher energy than infrared spectroscopy (Lourenço et al., 2012).

On-line UV-Vis spectroscopy is one of the methods which are currently used to monitor and control wastewater treatment plants. In fact, this method can be used to monitor both the influent and the effluent, determining the load of organic material (COD), nitrate and suspended solids (TSS), and also to control unique steps in the treatment process (for example aeration). On-line effluent monitoring is very helpful for meeting treatment process demands and subsequent wastewater discharge into the environment and it also serves to evaluate the effectiveness of this process (van den Broeke et al.,

2006). But despite the fact that the meeting legal discharge demands is the major driving force for wastewater quality monitoring, it information regarding the quality and quantity of the influents to a wastewater treatment plant is also required for its design and operation. Studies, based purely on visual observation and direct collation of UV-Vis spectra, have been reported. Nevertheless, data analysis for knowledge extraction regarding spectra from environmental samples is generally conducted using multivariate statistical methods, especially principal component analysis (PCA). In fact, it was reported that UV-Vis spectra of wastewater samples included information which, after extraction with PCA, was used for quality monitoring (Lourenço et al., 2006).

2.6 Chemometric processing of spectral information

Chemometrics is the science that takes measurements on chemical systems and describes the latter via the application of mathematics or statistics to those measurements. The aim of the majority of chemometric methods is the creation of empirical models, based on the obtained data, which served to estimate values for one or more properties of the measured system. Therefore this science is data-based (Wise and Gallagher 1996). The advantage of chemometric methods is their ability to facilitate the interpretation of certain chemical phenomena or its causes information that would not be obvious without this processing (Eckschlager 1991).
Principal component analysis (PCA) and Partial least squares (PLS) are examples of chemometric methods, which were used in this work.

2.6.1 Principal Component Analysis (PCA)

Principal component analysis (PCA) represents one of the most popular multivariate statistical methods, which can be used across nearly all scientific fields and which is probably the oldest multivariate method.
Principal Component Analysis (PCA) aims at the transformation of the raw data system into a more relevant one and the decrease of the original system's dimension by using a limited number of principal components (PC's) which reflect the structure of the data. A principal component model is an approximation to a given data matrix X (i.e., a model of X) to be used instead of the complete raw data. The model may be defined as:

$$X(n \times p) = T(n \times d)L^T(d \times p) + E(n \times p)$$

where *n* is the number of samples, *p* is the number of variables (wavelengths, for spectral data) and *d* is the number of PCs. *T* is the scores matrix, *L* the loadings matrix, L^T the transposed loadings matrix and *E* the residuals matrix.

For the specific instance of spectroscopic data, PCA determines the main sources of correlated variance in the original set of spectra through defining a series of PCs or factors, orthogonal to each other. It also gives to each original spectrum a score, representing its relative participation in each PC. Thus the original data set may be reduced from a multidimensional space to a representation called a score plot, which is a simpler visualization of the data in a two- or three-dimensional space. These score plots describe a major part of the information contained in the data and allow the visualization of their main trends (Lourenço et al., 2006).

The main goals of this analysis are the extraction of the most important information from the data set, the compression of the data set by considering only mentioned important information, the facilitation of the description of the data set and analysis of the structure of the measurement and the variables (Abdi and Williams, 2010).

Then PCA further enables the visualization of similarities between observations and correlations among the original variables by displaying them as points and vectors, respectively, in two- or three-dimensional charts, called bi-plots (Abdi and Williams 2010).

2.6.2 Partial least squares (PLS)

Partial least squares (PLS) regression is a method based on the principle of multiple linear regression. The absorbance values over the whole range (or part of it) of wavelengths in the measured spectra of samples are used in the PLS algorithm to create the calibration model, instead of absorbance readings at individual wavelengths (e.g., the maximum in a given range). The PLS method searches for set of factors (latent variables), which describe the distribution of both spectral data and analytical values for the same samples, maximizing the degree of covariance between them. This leads to the minimization of problems caused by cross-correlation between readings at different wavelengths.

All-important spectral and concentration information are condensed into sets of new latent variables during PLS calibration. Each component represents an independent source of variability in the calibration data set. These variables are sorted by the fraction of the data set variability they represent and the most important of them to be retained in the model is chosen to provide the best correlation between the analytical information and its correspondent spectral information (Beebe et Kowlaski 1987; Haaland et Thomas 1988a,b).

The PLS algorithm has become one of the dominant methods for multivariate calibration attesting the high quality of the resulting models (Venkatesan et al. 2011).

2.7 Thesis objectives and presentation

According to the objectives outlined in chapter 1, this thesis is presented into two parts. The first part was focused on the operation of three sequencing batch reactors (SBRs) with aerobic granular sludge (AGS) and the evaluation of their performances through off-line monitoring of operational parameters,

namely, suspended solids, and COD and color removal. These parameters were evaluated in samples, which were collected during selected SBR cycles.

The second part reports on results from the spectroscopic analyses of different aqueous solutions containing the components of the SBR feed. UV-Vis spectroscopy measurements were done on solutions of silver nanoparticles at various concentrations in milli-Q water, as well as combinations of nanoparticles with different concentrations of dye, starch-based substrate, the latter two together, minerals and finally the complete SBR feed solution. The acquired spectra were processed using chemometric methods, namely, PCA and PLS, for qualitative process monitoring and for key parameter quantification, respectively.

3. MATERIALS AND METHODS

3.1 Culture media

The reactor culture medium consisted of two parts. Part one the source of nitrogen (feed-N) and part two contained the source of carbon (feed-C).

Feed-C was composed of the carbon source and macronutrients, as shown in Table I, in which their final concentrations in the reactor are listed.

Table I – Composition of feed-C.

Compound	Concentration [mg.L^{-1}]
$MgSO_4.7H_2O$	22,5
$CaCl_2$	27,5
$FeCl_3.6H_2O$	0,25
Emsize E1 (from a stock solution)	1150

Hydrolyzed Emsize E1 (starch-based size agent, Hoechst Portuguesa, S.A) was used as carbon source. The stock solution (100 g L^{-1}) was prepared by dissolving NaOH (40 g) and Emsize E1 (100 g) in a distilled water (± 500 ml). Then it was left to hydrolyze at room temperature during at least 15 hours, after which its pH was adjusted to 7 with HCl 37% and its volume was finally adjusted to 1 L with distilled water. The solution was stored at 4ºC until use.

Feed-N was composed of the nitrogen source, phosphate buffer and micronutrients, as shown in Table II, in which their final concentrations in the reactor are listed.

Table II – Composition of feed-N.

Compound	Concentration [mg.L^{-1}]
$Na_2HPO_4.12H_2O$	2310
KH_2PO_4	762
NH_4Cl	143
Azo dye	40
$MnSO_4.4H_2O$	0.04
H_3BO_3	0.057
$ZnSO_4.7H_2O$	0.043
$(NH_4)_6Mo_7O_{24}.4H_2O$	0.035

The two feeds were mixed together to produce a synthetic wastewater with a chemical oxygen demand (COD) value of 1000 mgO_2 L^{-1}, which was used as the feed solution for the reactors. The COD:N:P mass ratio in this feed solution was 100:3.7:3.7.

Acid Red 14 was selected to represent the most common dye group used in the textile industry, azo dyes. Its stock solution was prepared by dissolving Acid Red 14 (Chromotrope FB, Sigma Aldrich Chemie GmbH, 50% dye content) in distilled water to the concentration of 5 g L^{-1}. The solution was

stored at 4ºC until use. The dye stock solution was added to the synthetic wastewater to a final concentration of 20 mg L^{-1}.

3.2 Inoculum

The inoculum used to seed the reactors in this study was a sample from a conventional activated sludge (CAS) bioreactor, which was obtained at the Chelas wastewater treatment plant (WWTP), Lisbon, Portugal.

3.3 Operation of the anaerobic-aerobic sequencing batch reactors

In this experiment three different anaerobic-aerobic sequencing batch reactors (SBRs) were operated at room temperature (approximately 23 °C). Two of these reactors (SBR1, SBR2) went through the fill stage while being mechanically stirred, while the third one (SBR3) was slowly filled by upward flow through the settled biomass bed at the bottom, without stirring (plug-flow type fill). At the drain stage, the settled effluent was drawn from the middle of the working reactor height. The exchange ratio of feed was thus 50% and the volumetric organic loading rate (ORL) was 2.0 kg COD m^{-3} d^{-1}. SBR1 and SBR2 were used to investigate the effect of the presence of silver nanoparticles (Ag-NP) in the feed on the formation of granules from flocculent sludge. Therefore, a stock suspension of nanoparticles (50 mg L^{-1}, in milli-Q water) was added together with the feed to SBR1, and SBR2 was used as an Ag-NP-free control. SBR3 was also free of Ag-NP and was used to examine the effect of the hydrodynamic feed regime (stirred *vs.* plug-flow).

Each reactor was filled with mixed liquor to the working volume of 1.5 L, giving a height/diameter ratio of 2.5.

The SBR operation consisted of cycles, each with a total duration of 6 hours. Each cycle was divided into six stages. At the beginning of each cycle the reactors were filled with 750 ml of wastewater (fill stage). The filling was followed by a reaction stage, which consisted of an anaerobic phase with mechanical stirring followed by an aerated (aerobic) phase (without mechanical stirring). After the aerobic phase, the settling stage began with the stopping of the aeration. From the beginning of the experiment, the duration of the settling stage was successively shortened from 1 hour to 40, 30, 20, 15, 10, and 5 minutes, to induce the formation of fast-settling biomass granules. The settling stage was followed by the drain stage and in the last part of the cycle the reactors were left idle. The duration of each stage is shown in Table III.

Table III – Duration of the SBR operational cycle stages.

Reactor	Fill	Reaction		Settling	Drain	Idle
		Anaerobic	Aerobic			
SBR 1/2	30 min	1.5 h	3.5 h	1h→5 min	1 min	-
SBR 3	1.5 h	30 min	3.5 h	1h→5 min	1 min	-

Mixing in the anaerobic phase was achieved with magnetic stirring at 70 ± 4 rpm for SBR1 and SBR2 and with motor drive mixing at 280 rpm for SBR3. Aeration was performed with air compressors through a membrane diffuser at the bottom of each reactor.

3.4 Preparation of the Ag-NP suspensions

The silver nanopowder was purchased from Sigma Aldrich Chemie GmbH. Considering the Ag-NP specification, the particle size was less than 100 nm, contained PVP as a dispersant and was 99,5% pure on a trace metals basis. The Ag-NP stock suspension (50 mg L^{-1}) used in the SBR1 feed was prepared by dispersing Ag-NP powder in milli-Q water and then applying sonication. The sonication was performed with a Sonopuls sonifier, model HD 3200 (Bandelin electronic GmbH& Co. KG, Germany), equipped with the TT13 probe at a power of 100 W for 30 minutes. Each sonication run consisted of successive cycles, 5 minutes on and 1 minute off, up to the defined total time. All Ag-NP suspensions, in different aqueous solutions, were subsequently prepared using this protocol.

3.5 Preparation of mixtures for spectral analyses

Mixtures were prepared in distilled water, with different concentrations of Ag-NPs, dye (AR 14), Emsize E1, and the minerals included in the synthetic SBR feed. Suspensions of Ag-NPs in water were prepared with concentrations of 2, 5, 10, 20, 50 and 100 mg L^{-1}. Then, combinations of 50 mg L^{-1} Ag-NPs were prepared either with Emsize E1, at concentrations of 0.1, 0.5, 1.15, 2 and 5 g L^{-1}, or with dye, at concentrations of 5, 10, 15, 20, 25 and 50 mgL^{-1}. Additionally, Ag-NPs at 50 mg L^{-1} were mixed in distilled water with both Emsize E1 (0.2875, 0.575, 0.8625, 1.15, 1.4375 and 2.875 g L^{-1}) and dye (5, 10, 15, 20, 25, 50 mg L^{-1}). Finally, Ag-NPs at 50 mg L^{-1} were mixed with the whole feed (WF) composition (Emsize E1, dye and minerals). UV-VIS spectra were acquired for all mixtures as described in section 3.7.4.

3.6 Chemometric analysis of spectral data

The data set generated from the procedure described in section 3.5 was composed of 70 spectra, each with 611 variables (absorbance readings at the measured range of wavelengths).

PCA analysis was performed with subsets from the spectral dataset, for selected sample groups, using mean-centered spectra. Univariate and multivariate PLS models for the prediction of the Ag-NP concentration from the spectra, were also developed with mean-centered spectra.

The PCA and PLS models were developed in MATLAB 7.4.0 (The Mathworks Inc., Natick, Massachusetts, U.S.A.) with the specific package PLS_Toolbox 3.0 (Eigenvector Research Inc., Wenatchee, Washington, U.S.A.).

The performance of PLS models was preliminarily assessed by using a leave-one-out cross validation procedure with the calculation of the root mean squared error of cross validation, RMSECV, as follows:

$$RMSECV = \sqrt{\frac{\sum_{j=1}^{n} (Par_j - Par_{M\,j})^2}{n-1}}$$

Where:

Par_j: parameter value of measured sample, for sample j.

$Par_{M\,j}$: parameter value estimated from the spectrum and model, for sample j.

n: number of samples

3.7 Sampling and analytical techniques

3.7.1 Bioreactor sampling

The samples for offline measurements were taken at six defined times during one of the SBR cycles (10h30 – 15h30), once a week. The sampling times are shown in Table IV.

Table IV – Scheduled sampling times during an SBR operational cycle.

Sample	SBR 1	SBR 2	SBR 3	Cycle stage	
1	10h30	10h30	11h30	Anaerobic phase	Start
2	11h00	11h00	-		During
3	12h00	12h00	12h00		End
4	12h30	12h30	12h30	Aerobic phase	Start
5	13h30	13h30	13h30		During
6	15h30	15h30	15h30		End
E	-	-	10h00		
F	-	-	11h30		

The mixed liquor sample volume taken from each reactor was 10 mL. After sampling, each tube was centrifuged (Eppendorf, model 5810 R, USA) to remove suspended solids. The centrifugation was performed at 4000 rpm for 10 minutes at 21 °C. After that 1 mL of the clear supernatant was collected into 1.5 mL eppendorf tubes for HPLC (in duplicates), 1.5 mL to glass tubes for COD analysis (in duplicate) and the rest of the supernatant was collected into 2 mL eppendorf tubes. The latter was used for UV-VIS absorbance and pH measurement and subsequently stored at -20 °C.

Samples from the feed (F) and the effluent (E) (Table IV) were also taken for SBR3. Offline analyses were carried out for total suspended solids (TSS), volatile suspended solids (VSS), chemical oxygen demand (COD), pH and UV-VIS absorbance.

3.7.2 Total suspended solids (TSS) and volatile suspended solids (VSS)

Total suspended solids (TSS) and volatile suspended solids (VSS) were measured in samples taken from the discharged effluent and from the SBR mixed liquor, in duplicate, at the end of the aerated phase. The dry residue ash content methods were used respectively, as described by Clescerl et al. (1999).

Glass microfiber filters (GF/C^{TM}, Whatman) with a diameter of 47 mm were used. Each filter was washed with distilled water in a vacuum filtration system, dried in a drying balance (model HB43-S halogen, Mettler Toledo), identified and treated in a muffle furnace (Program controller S27, Nabertherm) for 1.5 hours, at 550 °C, for the elimination of any organic residue. After that the filters were cooled and finally weighed in an analytical balance (model AE 160, Mettler).

Samples of 20 mL from the mixed liquor and of 10 mL from the mixed effluent were taken with glass pipettes (in duplicate for each reactor), and filtered through the prepared filters, in the vacuum filtration system. The filters with samples were dried in the drying balance, weighed in the analytical balance, calcined in the muffle furnace and weighed again in the analytical balance. Each weight was registered.

TSS was determined from the difference between the weight of the filter with sample after drying in the drying balance and that of the empty filter, divided by the filtered volume of sample. VSS was determined from the difference between the weight of the filter with sample after drying in the drying balance and after calcination in the muffle furnace, divided by the filtered volume of sample. The VSS/TSS ratio (%) was calculated dividing the concentration of VSS by the concentration of TSS and multiplying by 100.

3.7.3 Chemical oxygen demand removal (COD)

Chemical oxygen demand (COD) measurements were performed twice for each sample. To a volume of 1.5 mL of sample, 1 mL of $K_2Cr_2O_7$ digestion solution and 2 mL of H_2SO_4 with $AgSO_4$ solution was added in test tubes. The tubes were covered, mixed and inserted in a block digester (Spectroquant TR 420, Merck, Germany) at 148 °C for two hours. The tubes were allowed to cool down to room temperature, after digestion. After that the content of each tube was transferred to a 50-mL erlenmeyer flask, previously washed twice with distilled water. A drop of ferroin solution was added and the dichromate in excess was titrated with a ferrous ammonium sulfate solution (FAS, 0.0125M). The titration end point was achieved when the color of the solution changed from yellow/green to deep orange.

This process was also carried out for a blank of distilled water and for the standard dichromate solution (1 mL of $K_2Cr_2O_7$ standard solution and 2 mL of concentrated H_2SO_4 diluted with distilled water). The COD value was calculated as follows:

$$COD\,(mgO_2.L^{-1}) = \frac{(A-B)\times M \times 8000}{mL\ of\ \ sample}$$

Where:

A: mL FAS used for blank.

B: mL FAS used for sample or standard.

M: molarity of FAS, determined from the titration of the $K_2Cr_2O_7$ standard solution.

The used COD tubes were cleaned with a special procedure. First a small volume of chromo-sulfuric solution (4.6 mL) was added to the tubes and left to stand for at least one hour. Then the tubes were washed twice with acid solution (3 mL, 20% H_2SO_4) and finally washed three times distilled water.

3.7.4 UV-VIS absorbance

UV-VIS absorbance measurements were performed in a Specord 200 spectrophotometer (Analytic Jena, Germany), in the wavelength range 190 - 800 nm, with a resolution of 1 nm. Simple absorbance readings at 317 nm were used to estimate the dye concentration, using a previously prepared calibration curve. All readings were done in quartz cuvettes with an optical path length of 10 mm, against a blank of distilled water. The volume measured was 600 μl and each sample was measured twice.

4. RESULTS AND DISCUSSION

4.1 Off-line SBR monitoring

Off-line monitoring was carried out for the three SBRs described in section 3.3. SBR1 was fed with synthetic textile wastewater supplemented with Ag-NPs, SBR2 was operated as the Ag-NP-free control of SBR1 and SBR3 featured a plug-flow fill regime without Ag-NPs in the feed. The three SBRs were seeded with flocculent activated sludge and were operated in order to promote the formation of aerobic granules. Off-line monitoring during granulation consisted of measurements of TSS and VSS, COD analysis and UV-Vis spectroscopy.

4.1.1 Total suspended solids and volatile suspended solids

The assessment of the amount of biomass during granulation was performed by measuring the values of TSS and VSS in samples collected from the mixed liquor of each SBR and also in samples of the corresponding discharged effluent (treated wastewater) along the experimental period. TSS represents the total amount of suspended solids. On the other hand, VSS represents the fraction of TSS that is volatile, corresponding approximately to the organic matter present in the solids. The ratio VSS/TSS indicates the quality of the solids, with high values indicating high organic matter content, i.e., mainly microorganisms.

Fig. 3 represents the evolution of TSS in SBR1, supplemented with Ag-NPs, and inSBR2, used as Ag-NPs-free control, for 38 days operation to promote granulation. As shown, the TSS values gradually increased in both reactors from an initial concentration of around 3 gTSS L^{-1} to above 8 gTSS L^{-1}. Despite the presence of nanoparticles, TSS values for SBR1 were higher (up to 9.2 gTSS L^{-1}) than those for the control SBR2 (up to 8.6 gTSS L^{-1}). This finding is positive in terms of the effect of the presence of Ag-NPs in SBR1 because it shows that Ag-NPs do not have a negative influence on biomass growth.

In terms of the treated wastewater, Fig.3 indicates that SBR2 had a larger portion of biomass washed out of the reactor between days 3 and 24 (around 1.5 gTSS L^{-1}), but at the end of the experimental time, TSS levels in the treated wastewater were comparable to the ones observed in SBR1 (0.17 gTSS L^{-1}).

The VSS/TSS values for these two reactors varied within the 77-91% range, with the highest VSS/TSS value (91%) determined for SBR1 on day 24.

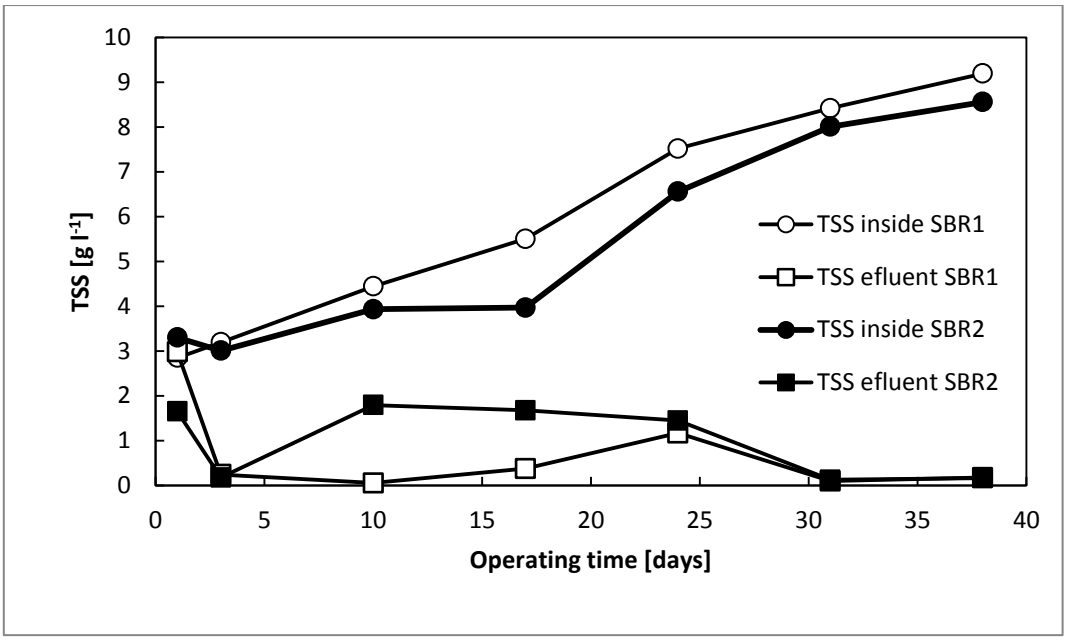

Figure 3– Biomass concentration (TSS) profile for SBR1, fed with simulated textile wastewater supplemented with Ag-NPs, and SBR2, used as Ag-NP-free control of SBR1.

The TSS concentration profile in SBR3 is shown in Fig. 4. Similarly to SBR1 and SBR2, the TSS concentration in SBR3 gradually increased, but without reaching the high levels observed in SBR1 and SBR2. In fact, TSS values lower than 7 gTSS L^{-1} were attained in SBR3 starting from an initial concentration of 3gTSS L^{-1}. The VSS/TSS values in SBR3 fluctuated between 78 and 88%. Discharge of biomass in the treated wastewater decreased from 4.6 to 0.07 gTSS L^{-1} throughout the granulation process. At the end of the experimental time, the effluent of SBR3 contained around half the amount of biomass of the other two bioreactors.

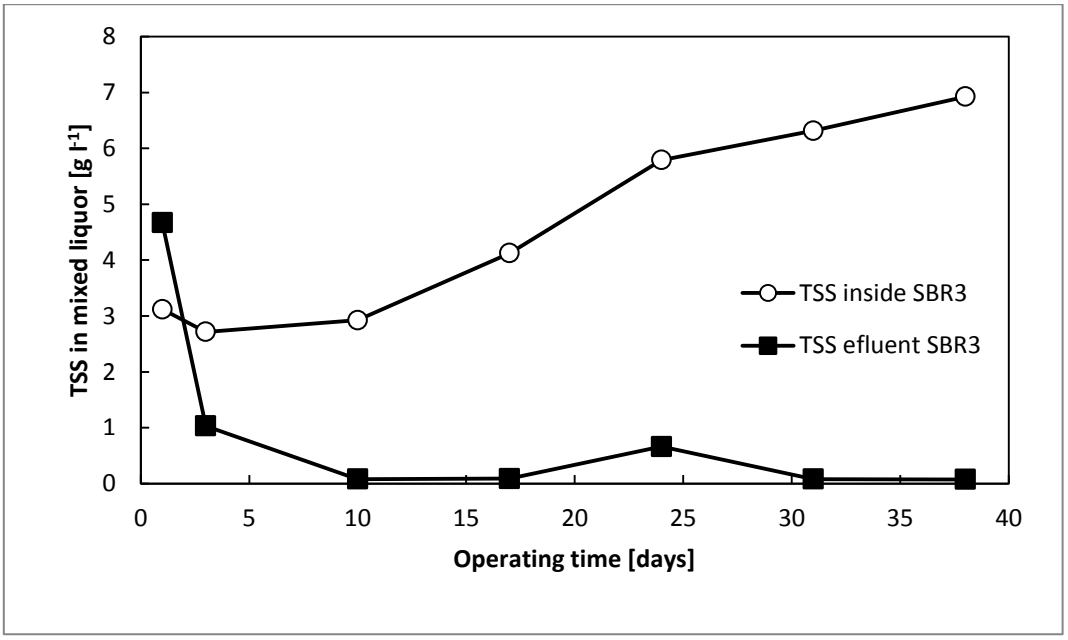

Figure 4 – Biomass concentration (TSS) profile for SBR3, operated under a plug-flow fill regime without Ag-NPs in the feed.

4.1.2 Chemical oxygen demand removal

The organic load removal performance of the AGS SBR system was evaluated by measurements of COD in samples collected from the mixed liquor of each SBR during selected treatment cycles along the experimental run, after clarification. In Fig. 5 the COD removal profiles of three cycles monitored during the first 10 days of operation for SBR1 and SBR2 are shown. Low COD removal levels were observed in first two monitored cycles in both reactors. This was probably due to the changes of feed composition, from domestic wastewater to the synthetic textile wastewater, and also due to changes in the operational strategy, from a continuous aerobic full-scale reactor to anaerobic-aerobic lab-scale SBRs. The COD removal levels in SBR1 observed in two first monitored cycles were higher (34 and 49%, respectively) than the COD removal levels of SBR2 (23 and 41%, respectively) despite of presence of Ag-NPs in the SBR1.

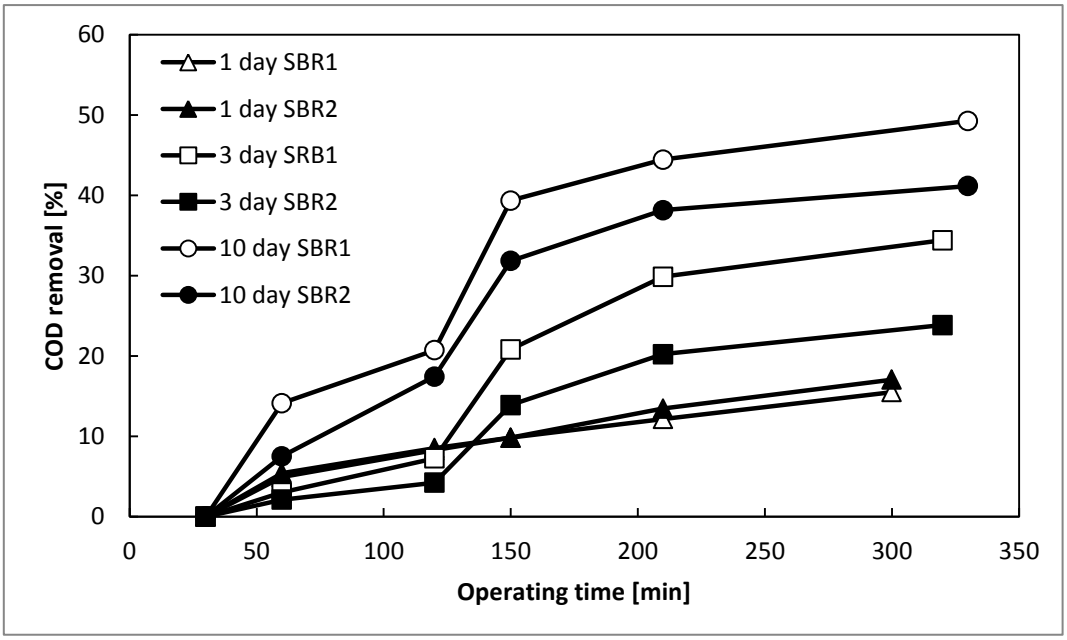

Figure 5 – COD removal profiles in monitored cycles of SBR1 and SBR2 along the first 10 days of operation.

But as is seen in Fig. 6, after two weeks of operation the differences between the COD removal profiles of the two SBR were attenuated due to adaptation of the biomass. So it can be suggested that Ag-NPs did not have a negative impact on COD removal. It can also be seen in Fig. 6 that after adaptation the COD removal levels increased up to 60% in SBR2 on day 31. Otherwise COD removal moved around 45% and with similar time profiles. On day 38, COD removal in SBR2 was lower (35%) than one may expect. This may be caused by shock from a change in the feed concentration, which has accidentally occurred during the previous cycle.

From Fig. 6, it is clear that COD removal occurred mainly in the anaerobic phase, whereas during the aerobic phase the COD values stayed almost unchanged.

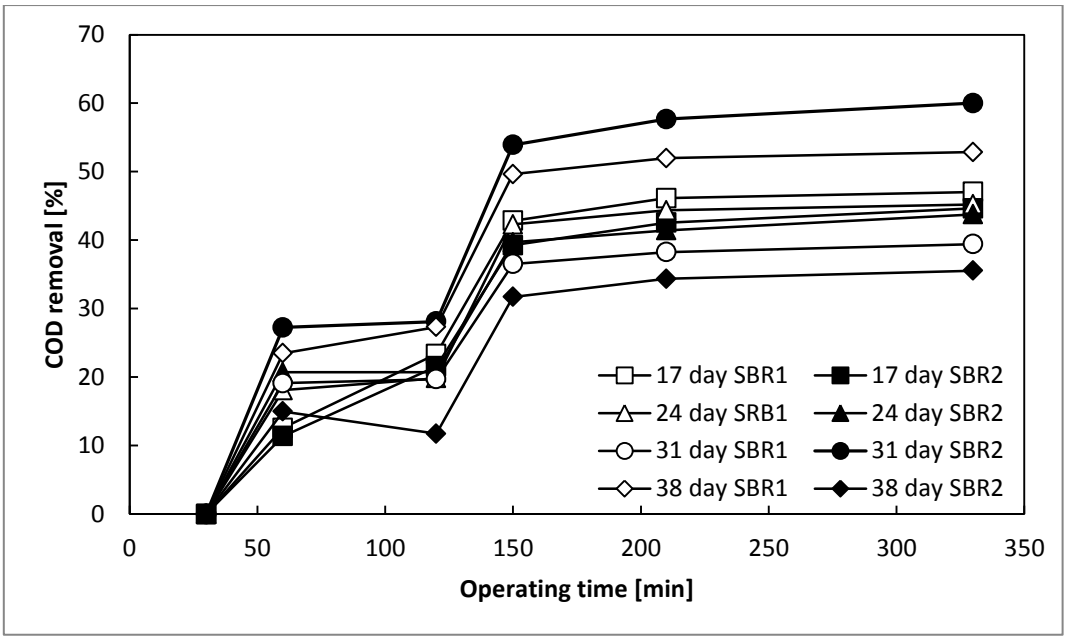

Figure 6 – COD removal profiles in monitored cycles of SBR1 and SBR2 along the 17-38 days of operation.

COD removal profiles for SBR3 are presented in Fig. 7. As seen, the COD removal profiles were similar to the ones observed in SBR1 and SBR2. The first two monitored cycles of SBR3 had also low COD removal efficiencies, 9 and 20%, respectively. But it increased to 40% along to the reported experimental period. And similarly to SBR1 and SBR2, COD removal took place mostly during the anaerobic phase. These results suggest that the different feeding regime of SBR3 did not have a negative impact on COD removal.

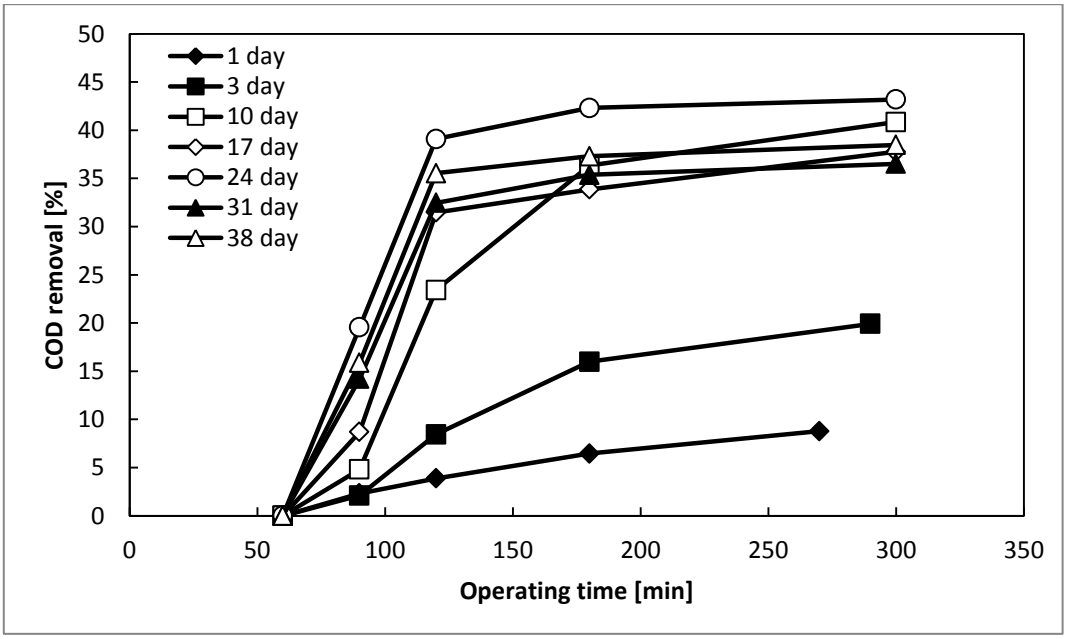

Figure 7 – COD removal profiles in monitored cycles of SBR3.

4.1.3 Color removal

Color removal profiles during SBR treatment cycles were obtained using UV-Vis spectroscopy to estimate azo dye (AR14) concentration. As seen from Fig. 8, the biomass rapidly adapted to the dye-laden synthetic wastewater. The dye concentration was stable only during the first reported cycle (day 1) for both SBRs (around 19 mg L^{-1} for SBR1 and 17 mg L^{-1} for SBR2). All subsequent cycles demonstrated a significant reduction of dye concentration, which is also evident in Fig. 9, where color removal profiles from day 17 on are shown for SBR1 and SBR2.

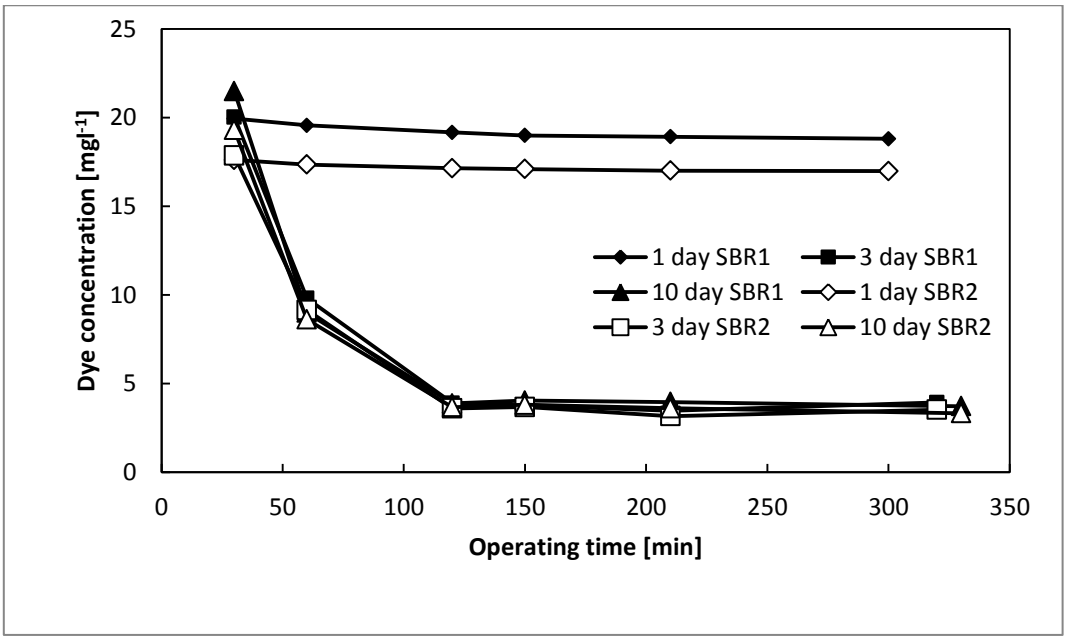

Figure 8 – Azo dye concentration in monitored cycles from days 1 to 10 for SBR1 and SBR2.

At the end of the treatment cycles from day 17 and day 24 the dye concentration in SBR1 was lower than in SBR2, as evident in Fig. 9. The lowest dye concentration achieved was around 2.5 mg L^{-1}, which corresponds to a dye removal level of 87.5%. It is also observed in Fig. 8 and Fig. 9 that dye removal took place during the anaerobic phase since dye concentration during the aerobic phase stayed almost unchanged.

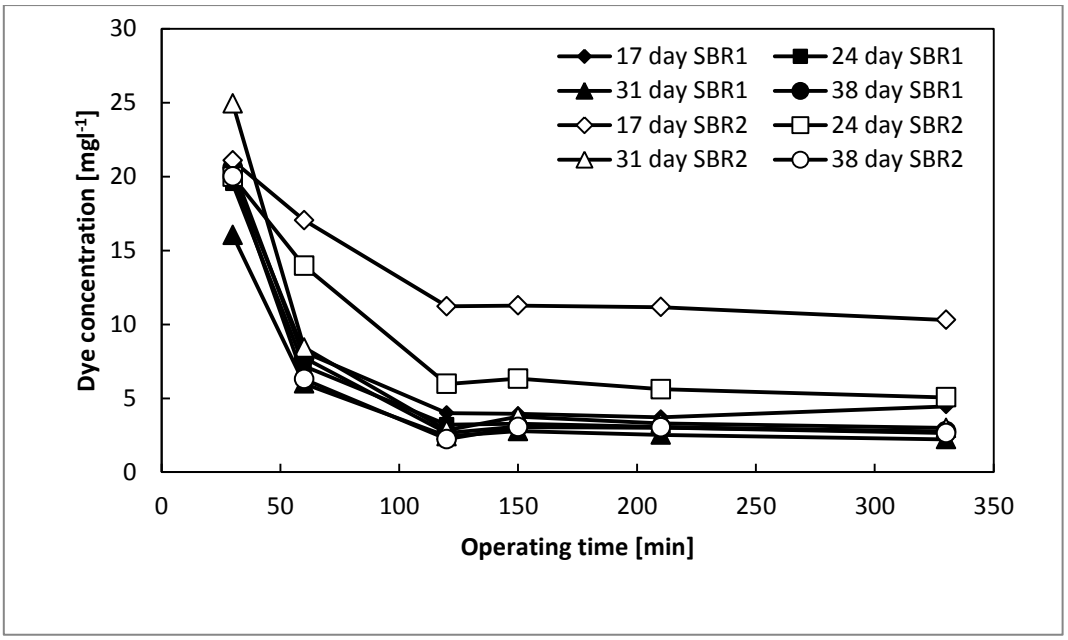

Figure 9 – Azo dye concentration in monitored cycles from days 17 to 38 for SBR1 and SBR2.

Color removal profiles for SBR3 are shown in Fig. 10. It is clear that reduction in dye concentration is not as large as in SBR1 and SBR2. This might be a consequence of the longer filling stage of SBR3 with a correspondent reduction of the anaerobic phase duration. Similarly to SBR1 and SBR2, color removal was not observed during the first monitored cycle of SBR3 (day 1). On the other hand, SBR3 presented a higher variability in color removal profiles than the other two SBRs. The lowest final dye concentration value in SBR3, 7.2 g L^{-1}, was measured on day 24, which corresponds to 64% color removal. These results show that SBR3, with its plug-flow feeding regime, is less effective for azo dye color removal than SBR1 and SBR2.

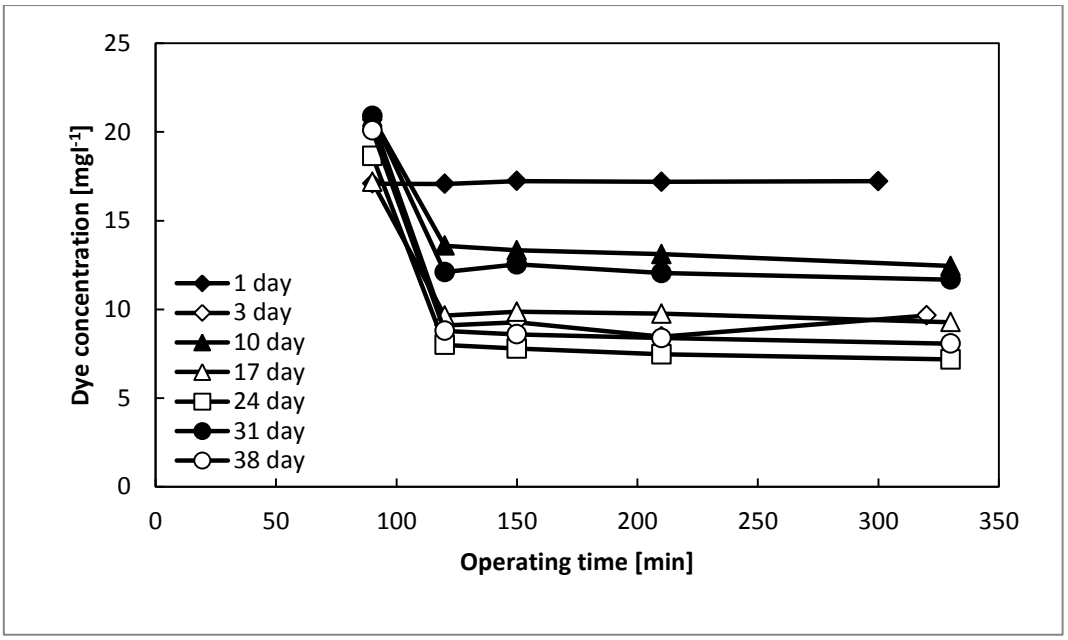

Figure 10 – Color removal profile in monitored cycles of SBR3.

4.2 Qualification of Ag-NP wastewater suspensions with Principal Component Analysis

4.2.1 UV-Vis spectra of Ag-NP suspensions

UV-Vis spectra of different Ag-NP suspensions were acquired as is described in the section 3.7.4. The more detailed summary of the different samples used for UV-Vis measurements is shown in the Table V.

Table V – Summary of the different Ag-NP suspensions analyzed.

Sample	Ag-NP [mg L^{-1}]	Concentration range [mg L^{-1}]	Content in distilled water
Ag-NP	2-100	2-100	Ag-NP
Dye	50	5-50	Ag-NP+Dye
Emsize E1	50	100-5000	Ag-NP+Emsize E1
Dye and Emsize E1	50	5-50 and 287,5-2875	Ag-NP+ Dye+Emsize E1,
Minerals	50	Proportionally to dye conc.	Ag-NP+Minerals
Whole feed (WF)	50	Proportionally to dye conc.	Ag-NP+ Dye+Emsize E1+Minerals

From the following three spectra (Fig. 11, Fig. 12 and Fig. 13) is obvious that it is not easy to identify the effect of wastewater components on the Ag-NP absorption band without more detailed analysis. In Figure 11 it is shown UV-Vis spectra of Ag-NPs with different dye concentrations, in Figure 12 the UV-Vis spectrum of Ag-NPs with different concentration of Emsize E1 and in Figure 13 it is shown the spectra of whole reactor feed (WF) .

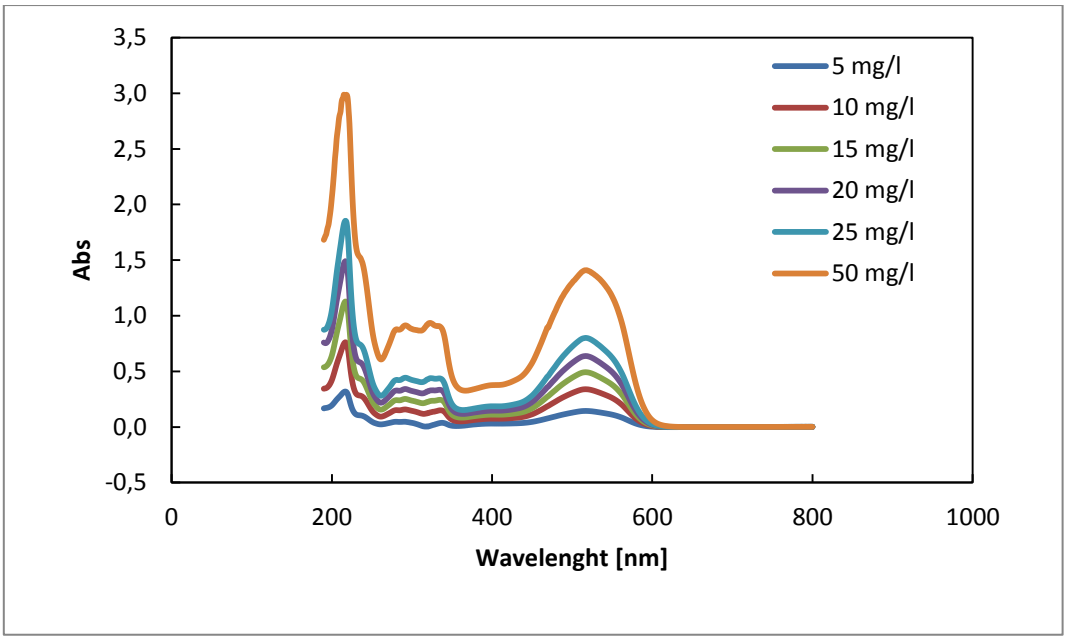

Figure 11 – Measured UV-Vis spectra of Ag-NPs (50 mg L^{-1}) with different concentration of the azo dye AR14.

It is visible on the graphs the absorbance decrease around the 300-400 nm wavelength range typical for Ag-NPs. However it is not clear what this region is affected with. Due to this insufficient resolution fact it is necessary to use more efficient methods of extraction of information such as, in this case, PCA.

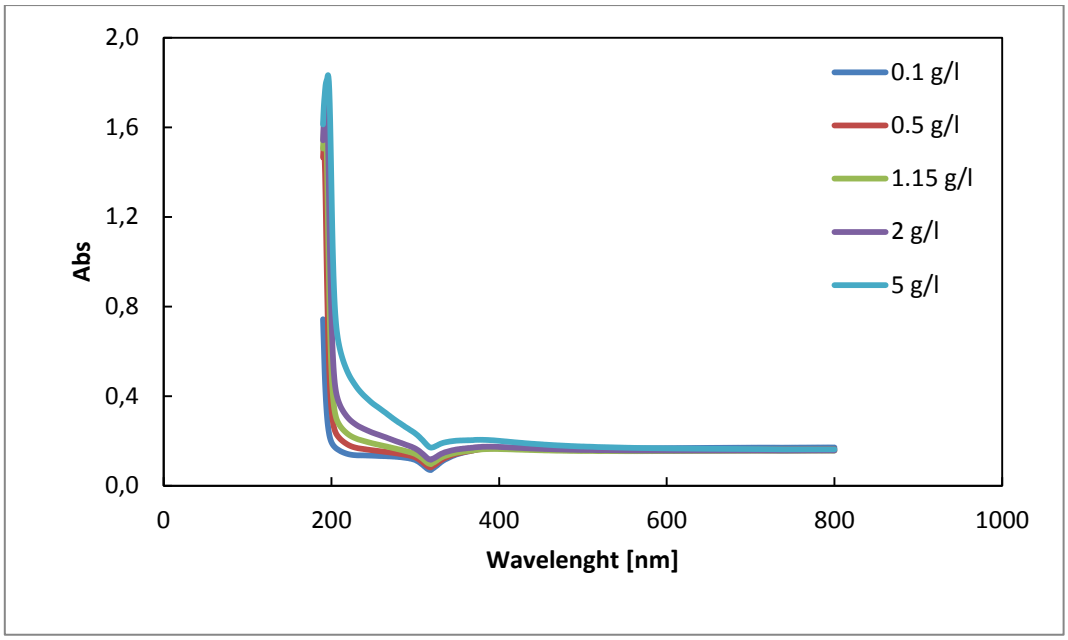

Figure 12 – Measured UV-Vis spectra of Ag-NPs (50 mg L^{-1}) with different concentration of Emsize E1.

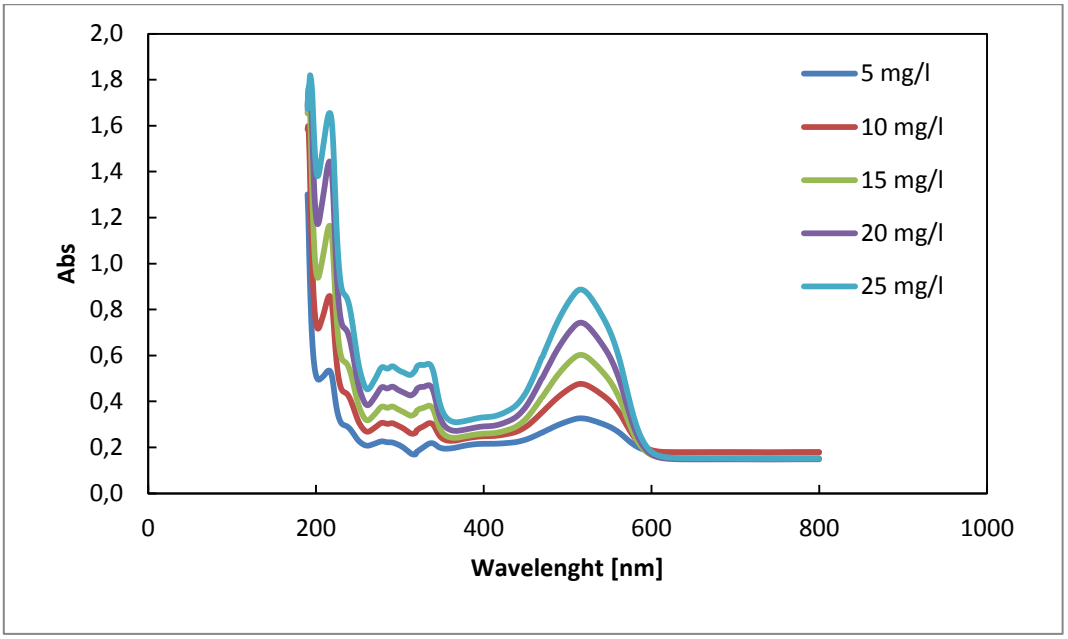

Figure 13 – Measured UV-Vis spectra of Ag-NPs (50 mg L^{-1}) with different concentration of whole reactor feed .

4.2.2 PCA model development

Principal component analysis (PCA) was carried out by using mean-centered UV-Vis spectra acquired from samples with various concentrations of Ag-NPs in distilled water and also Ag-NPs in distilled

water in the presence of different concentrations of AR14, Emsize E1, both AR14 and Emsize E1, minerals (included in the feed solution) and complete feed solution.

In a PCA model, the number of principal components represents a measure of data complexity and it may be considered as the number of independent basic phenomena. Therefore, a suitable selection of the number of components number is necessary. In this work, the number of relevant PCs to include in the PCA models was selected based on the analysis of the variance captured by each PC (Lourenço et al. 2006), complemented with the analysis of the eigenvalues in ascending order of magnitude, looking for a noticeable jump in these values.

Six PCA models were developed using UV-Vis spectra of Ag-NP suspensions to assess the influence of other compounds of the bioreactor feed (synthetic wastewater) on the spectra of these suspensions. The first model (PCA1) was developed with spectra from all the samples described in table V in the wavelength range of 190-800 nm. Based on the variance captured by the PCs (Fig. 14) it was decided to use three PCs in PCA1. These PCs captured 98.59% of total variance present in the dataset (91.75%, 4.83%, 2.01% and for PC1, PC2 and PC3, respectively).

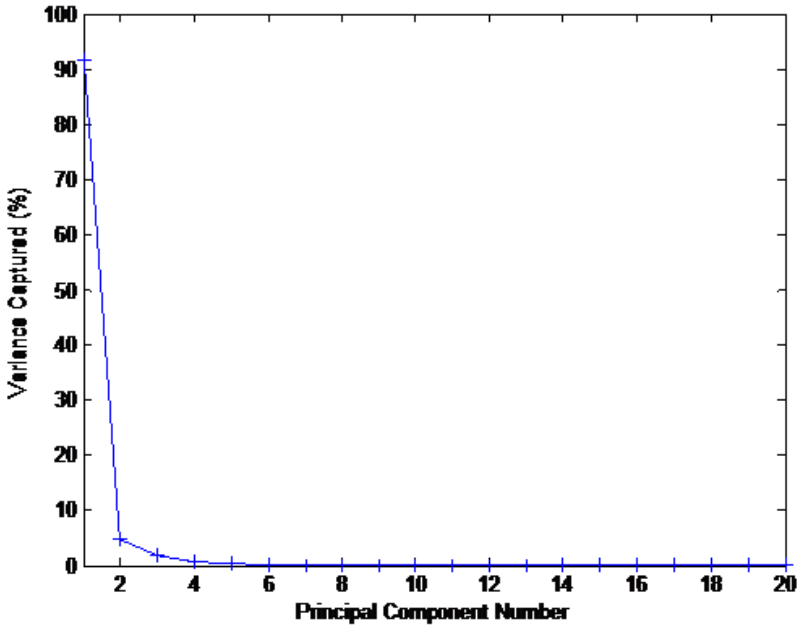

Figure 14 – Variance captured by each PC using mean centered spectra of synthetic wastewater samples containing Ag-NPs.

In the second model (PCA2, 3PCs) all the acquired spectra were used apart from those of samples with dye concentration of 50 mg L^{-1}, due to their noticeable difference from the other spectra. The third model (PCA3, 2PCs) was developed using a smaller range of wavelengths (250-400 nm), which corresponds to the region reported as typical for Ag-NP suspensions. The fourth model (PCA4, 2PCs) was also developed using the 250-400 nm wavelength range, but excluding spectra of samples corresponding to an azo dye concentration of 50 mg L^{-1}. The last two models, PCA5 (2 PCs) and PCA6 (2 PCs) were developed using the 250-800 nm wavelength range of in order to eliminate the

impact of the first large absorbance band appearing in the spectra. PCA6 was developed without spectra from samples containing AR14 in the concentration of 50 mg L^{-1}.

4.2.2.1 PCA1 and PCA2 model interpretation – vector loadings, scores plot and Q residuals

A loadings plot gives information on the interrelationships of original variables. One-vector loading plots are typically used for interpretation of spectroscopic data, since they often resemble spectral properties (Lourenço et al, 2006).

In Fig. 15 it is shown the one-vector loading plot corresponding to PC1 of PCA1 model in comparison with the normalized UV-Vis spectrum of a 20 mg L^{-1} AR14 dye solution. It can be seen that PC1 presents a profile similar to the UV-Vis spectrum of AR14. The vector-loading of PC1 also contained a significant absorption band around 515 nm, which is typical for in UV-Vis spectra of AR14 solutions in distilled water. Thus, it can be suggested that in PCA1, PC1 contained information related to dye concentration. The same was also observed for PCA2 (data are not shown).

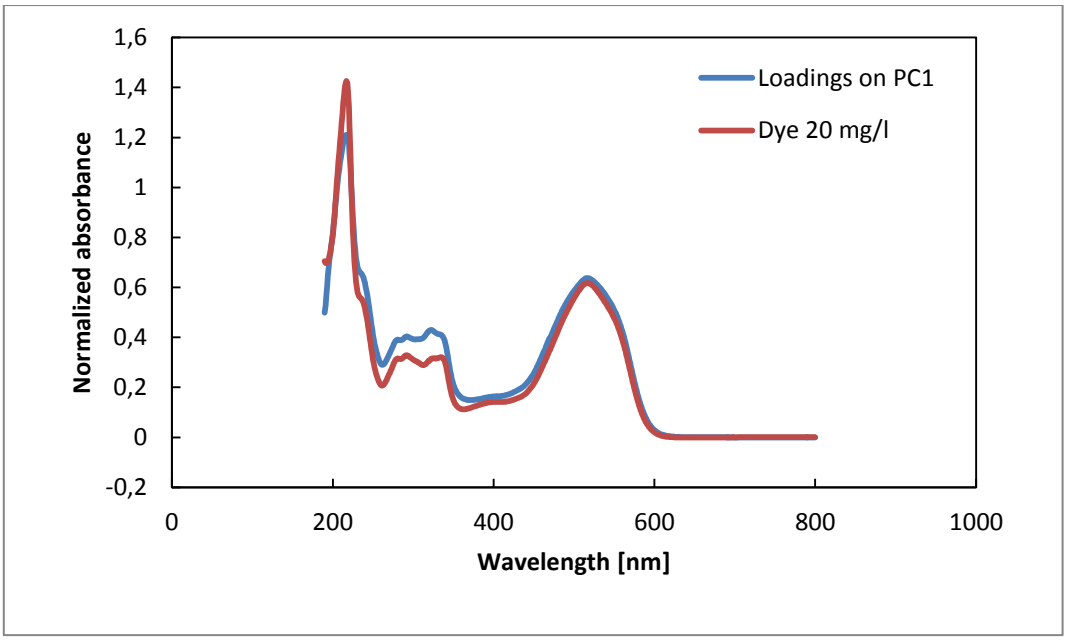

Figure 15 – One-vector loading of PC1 for PCA1 model in comparison with a normalized spectrum of a 20 mg L^{-1} AR14 solution in distilled water.

The one-vector loading plot corresponding to PC3 of PCA1 model is presented in Fig. 16 in comparison with the normalized UV-Vis spectrum of a 50 mg L^{-1} Ag-NP suspension in distilled water. From Fig. 16, it may be presumed that PC3 in PCA1 contains information related to Ag-NP concentration due to the absorbance decrease observed around the 300-400 nm wavelength range of. This was also observed for PC3 of PCA2 model (data not shown).

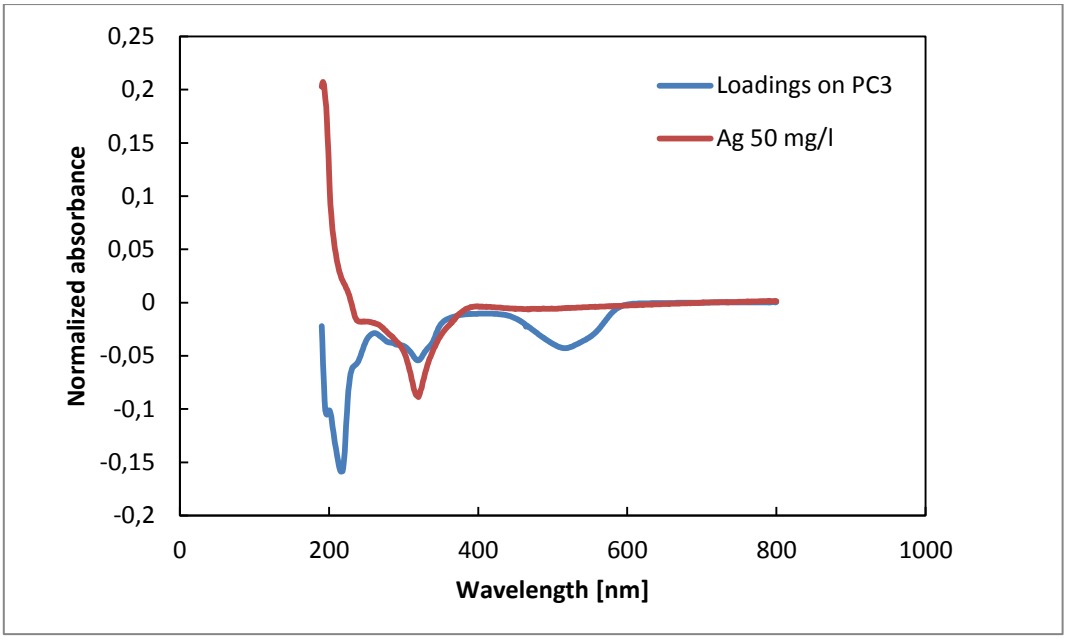

Figure 16 – One-vector loading of PC3 for PCA1 in comparison with a normalized spectrum of a 50 mg L^{-1} Ag-NP suspension in distilled water.

As shown in section 4.2.1, the analysis of differences and relationships between UV-Vis spectra by direct visual comparison might be challenging. However, these features can be evaluated in a scores plot, which shows the details about the relationship between individual samples. In a scores plot, two score vectors are plotted against each other. Individual samples are represented as a data point, with similar samples appearing close in the plot (Lourenço et al. 2006).

The scores plot for PC1 and PC2 of PCA1 model is shown in Fig. 17. The percentage of the total variance captured by these two PCs was 96.58% (91.75% for PC1, 4.83% for PC2). Four different groups of samples may be highlighted in Fig. 17. Group 1 corresponds to samples of Ag-NP suspensions in distilled water. Group 2 includes samples with fixed Ag-NP concentration and different AR14 concentrations. Group 3 corresponds to Ag-NP suspensions with different minerals and Emsize E1 content. Group 4 consists of Ag-NP suspensions in the complete bioreactor feed or in AR14 with Emsize E1 solutions. The two samples (duplicates) there are not included in the described groups correspond to Ag-NPs suspended in a 50 mg L^{-1} AR14 solution, both in the presence or in the absence of Emsize E1. Therefore, a new PCA model (PCA2) was developed excluding these samples.

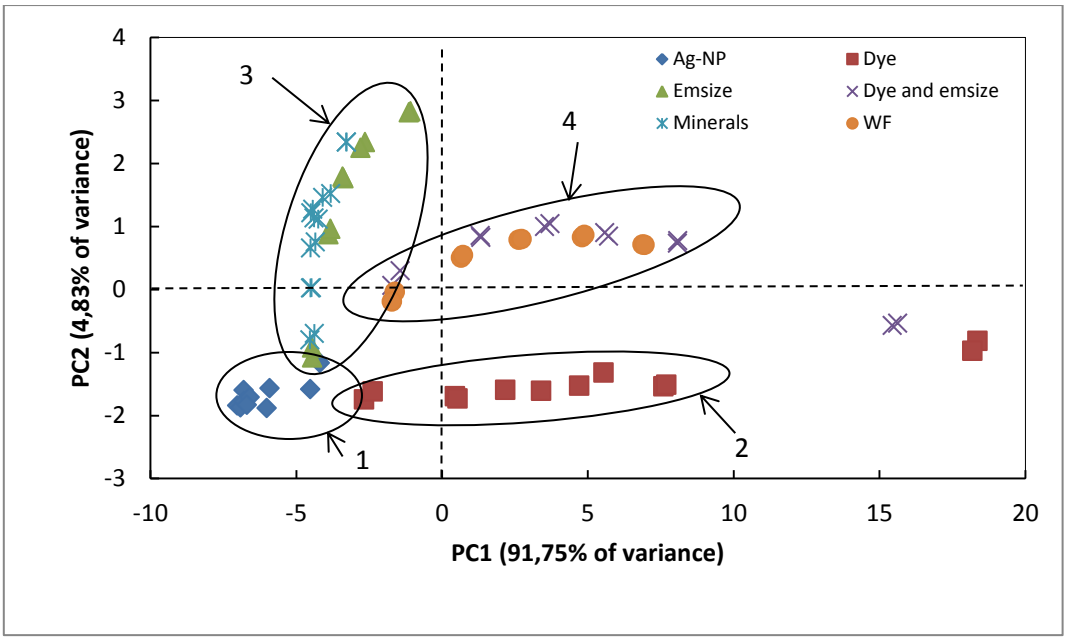

Figure 17 – Scores plot of PC1 and PC2 from PCA1 model.

From Fig. 17 it can be suggested that that dye concentration is correlated to PC1, since samples with increasing dye concentration (group 2) present increasing score values in PC1. On the other hand, the scores of PC2 stayed almost unchanged for these samples and the same was observed for Ag-NP suspensions in distilled water (group 1), which suggests that PC2 does not include relevant information regarding Ag-NP concentration. It can also be observed in Fig. 17 that samples with increasing Emsize E1 and minerals concentration (group 3) present increasing score values in PC2. However, these samples are not so significantly separated along PC1, similarly to Ag-NP suspensions in water (group 1). In fact, significant variations in the scores of both PC1 and PC2 were not observed for Ag-NP suspensions in water. When Ag-NPs were mixed with a dye solution the scores shifted toward positive values along the PC1 axis and after being mixed with Emsize E1 or mineral solutions the scores shifted toward positive values in PC2.

The same observations were achieved for PCA2 (results not shown), where the samples with AR14 concentration of 50 mg L^{-1} were excluded. The main differences between PCA1 and PCA2 models were in terms of the individual percentage of variance captured by each PC. For PCA1, as is shown in the Fig. 17, it was 91.75% for PC1 and 4.83% for PC2. For PCA2 it was 86.87% and 8.59% for PC1 and PC2, respectively. This indicates that the first two PCs of PCA1 represent better the dataset (96.58%) then PCA2 (95.46%).

The scores plot of PC1 and PC3 of PCA1 model is presented in Fig. 18. It can be seen that the samples with increasing Ag-NP concentrations in water are located along the PC3 axis, suggesting that this PC contains information related to Ag-NPs. The suspensions containing AR14 were separated along the PC1 axis as in Fig. 17. However, on the contrary to Fig. 17, the samples with minerals are clustered together in Fig. 18. It can also be seen that with increasing Emsize E1 concentration, the score values of PC3 decreased. In Fig.18 three samples (with duplicates) were really different from the others, corresponding to the suspensions with 50 mg L^{-1} AR14 as in Fig. 17

and also to the samples with the highest Ag-NP concentrations in water (100 mg L^{-1}). These differences were probably caused by a higher component concentration than in other samples.

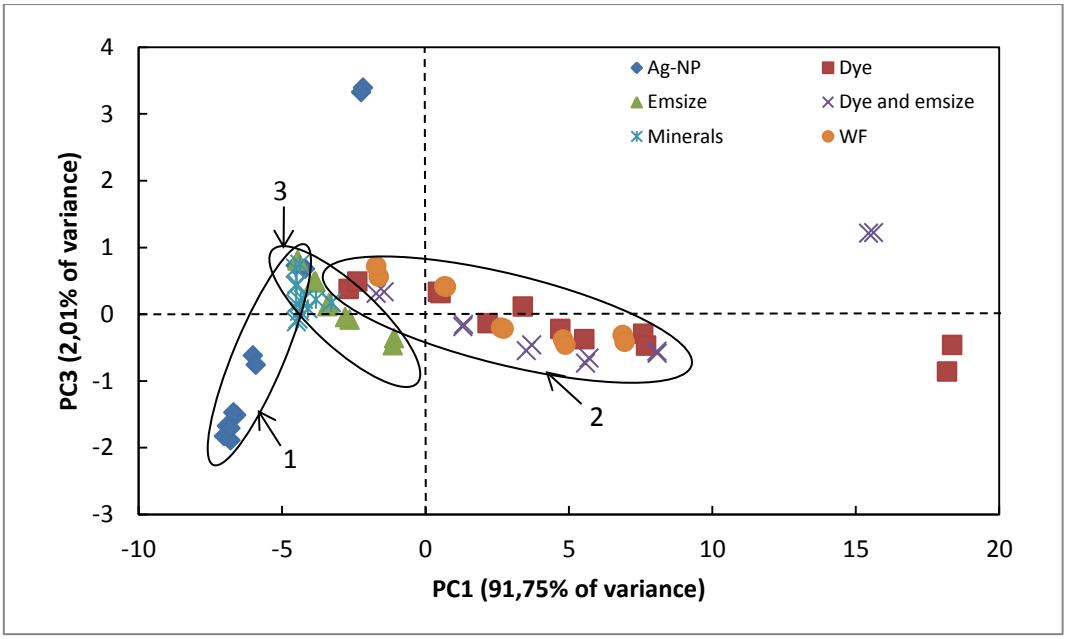

Figure 18 – Scores plot of PC1 and PC3 from PCA1 model.

Similar results were attained for the PCA2 model but with a higher variance captured by PC3 (2.01% and 3.52% for PCA1 and PCA2, respectively). Thus, the elimination of the samples with a dye concentration of 50 mg L^{-1} resulted in an increase of the variance captured by PC2 and at the expense of PC1.

Q statistic indicates how well each sample corresponds to the PCA model (variations outside the model). In other words, it is the measure of residuals between the sample and its projection into the PCs retained in the model. It can be plotted against the sum of normalized squared scores, named Hotelling's T^2 statistic. The latter describes the variation in each sample within the PCA model, i.e., variation inside the model (Shaver et al. 2005).

The Q residuals against Hotelling's T^2 were represented for PCA1 (Fig. 19) and also for PCA2 (Fig 20). In Fig. 19, it is evident that all the samples had a relatively similar behavior, apart from the previously mentioned samples corresponding to Ag-NP suspensions in 50 mg L^{-1} dye solution and samples of suspensions containing 100 mg L^{-1} AG-NPs in water. On the other hand, samples corresponding to Ag-NPs suspended in 5 g L^{-1} Emsize E1 solution were not well described by the PCA1 model. Similar results were obtained for PCA2 (Fig. 20). The Q residual limits for PCA1 and PCA2 were 0.55% (Fig. 19) and 1.02% (Fig. 20), respectively.

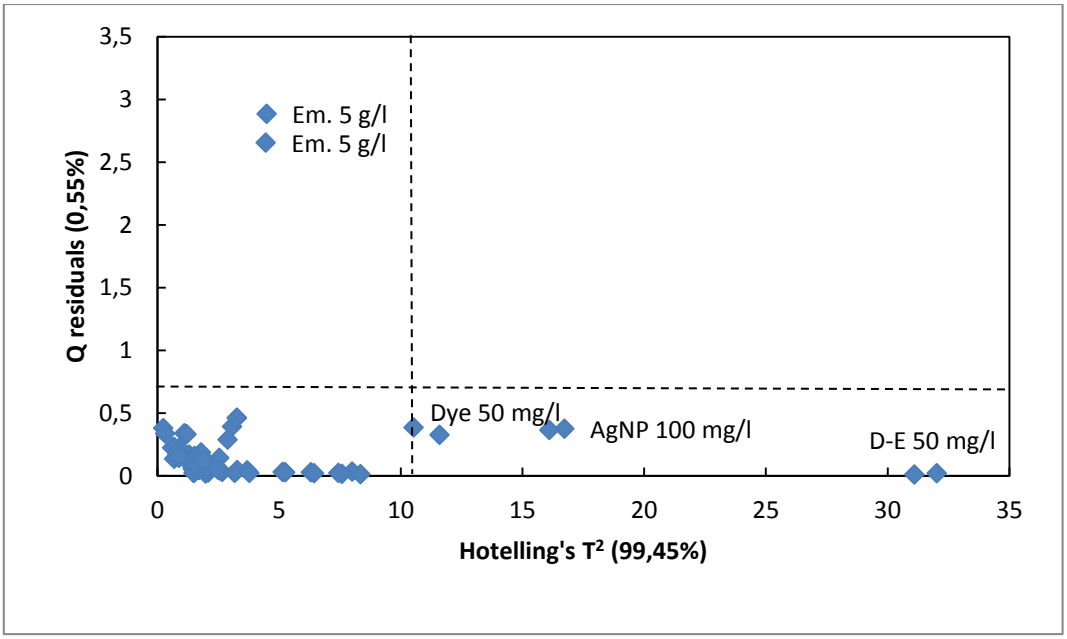

Figure 19 – Hotelling's $T^2$and Q residuals for PCA1 model

According to the plot of Fig. 19, most of the samples were in Q range 0-0.5 % and Hotelling's T^2 range 0-5. However, three samples (Ag-NP suspensions in 50 mg L^{-1} AR14 and in 50 mg L^{-1} AR14 and Emsize E1 and 100 mg L^{-1} Ag-NPs in water) were well described by the PCA1 model, but they were significantly different from the others. On the other hand, one of the samples (Ag-NPs in 50 g L^{-1} Emsize E1 solution) was poorly described by the model with Q residuals of 2.7%.

In Fig. 20, after excluding the samples containing 50 mg L^{-1} AR14, their distribution became more visible, with most of the samples presenting Hotelling's T^2 values in the 0-4 range. The sample with 100 mg L^{-1} Ag-NPs in water and the sample with AG-NPs in 5 g L^{-1} Emsize E1 solution presented a similar behavior as described for PCA1.

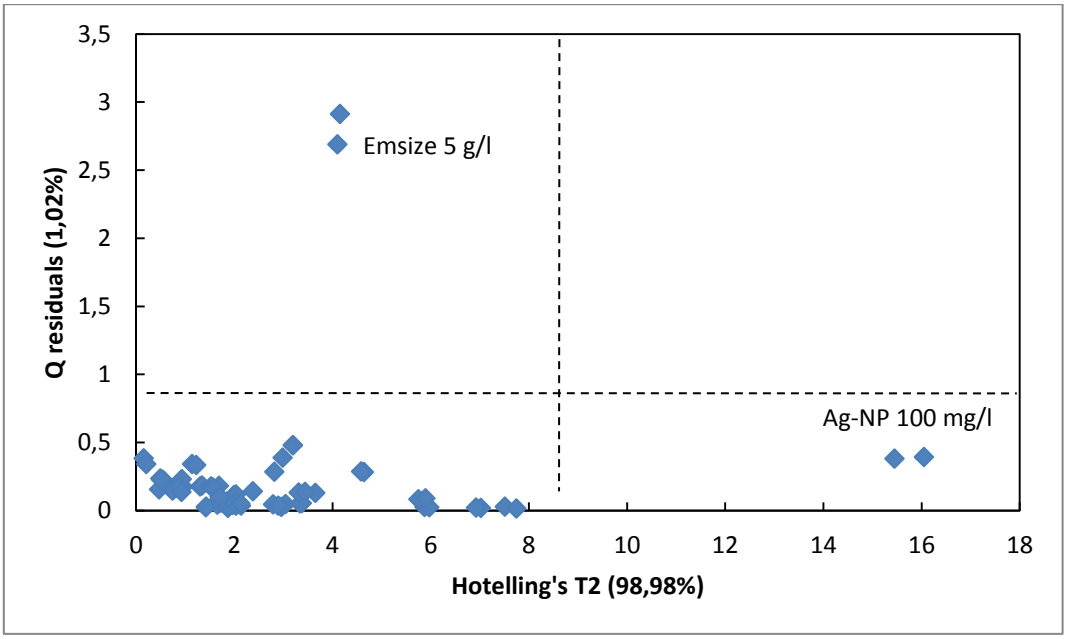

Figure 20 – Hotelling's $T^2$and Q residuals for PCA2 model

4.2.2.2 PCA3 and PCA4 model interpretation – vector loadings, scores plot and Q residuals

In Fig. 21 it is shown the one-vector loading plot corresponding to PC1 of PCA3 model in comparison with the normalized UV-Vis spectrum of a 20 mg L^{-1} AR14 dye solution. PC1 had very similar properties to the UV-Vis spectrum of AR14, suggesting that in PCA3, PC1 contained relevant information related to dye concentration. In fact, the one-vector loading of PC1 contained a significant absorption band around 515 nm, which is typical for UV-Vis spectra of AR14 solutions in water. This plot was very similar to the plot showing loading on PC1 for PCA1 model (Fig 15). The same results were also recorded for PCA2 (data not shown).

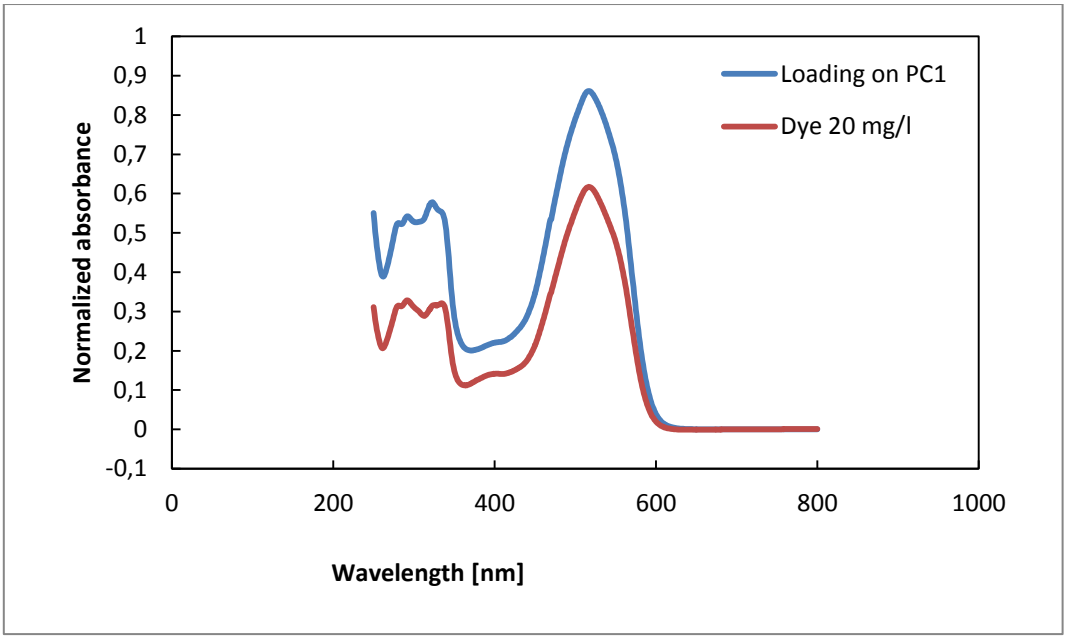

Figure 21 – One-vector loading of PC1 for PCA3 in comparison with a normalized spectrum of a 20 mg L^{-1} AR14 solution in distilled water.

In Fig. 22, the resemblance of the one-vector loading plot corresponding to PC2 and the normalized UV-Vis spectrum of a 50 mg L-1 Ag-NP suspension in water is shown. An absorbance decrease was observed around the 300-400 nm wavelength range, suggesting that PC2 contained information related to Ag-NPs. The same trend was also demonstrated in the PCA4 model (not shown).

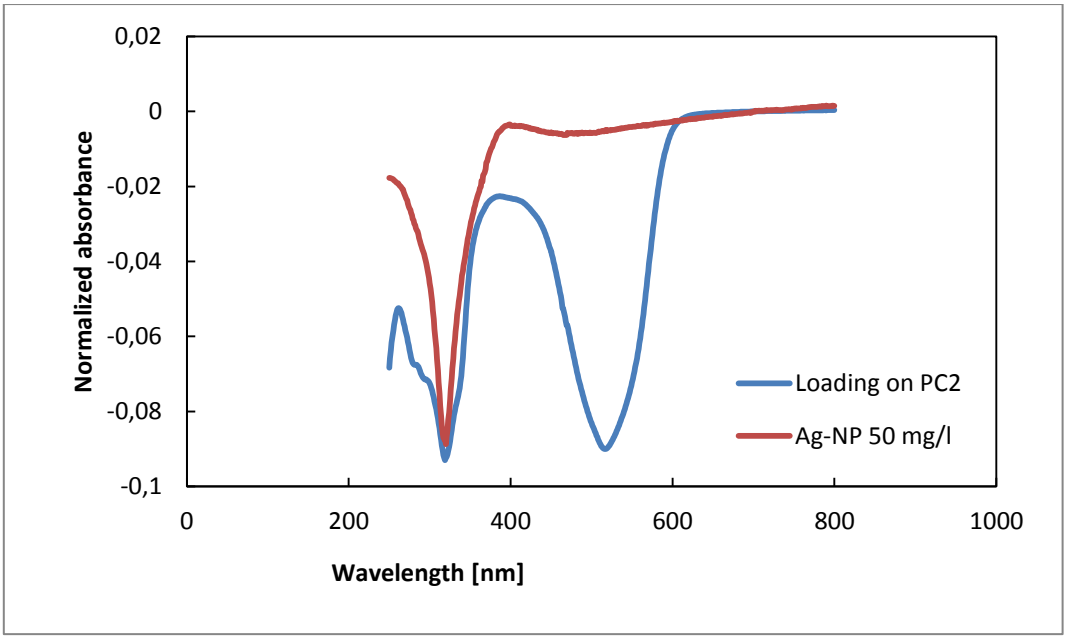

Figure 22 – One-vector loading of PC2 for PCA3 in comparison with a normalized spectrum of a 50 mg L^{-1} Ag-NP suspension in distilled water.

The scores plot for PC1 and PC2 of PCA4 model is presented in Fig. 23. In this model, sixty variables corresponding to the UV wavelength region were excluded in order to evaluate the effect of this wavelength region in the results. Similar results were obtained for PCA3 (data not shown) but the scores plot is easier to interpret excluding the samples corresponding to Ag-NP suspensions in 50 mg L^{-1} AR14 (PCA4) and only this plot is presented. Three groups of samples could be identified in Fig. 23. The first group (1) included samples of Ag-NP suspensions in water. In comparison with the scores plot of Fig. 17, it is shown that in PCA4, PC2 contained more information related to Ag-NP concentration. In fact, samples with increasing Ag-NPs concentration are distributed along the PC2 axis in the positive direction. This phenomenon is apparently due to the omission of absorbance values for the initial wavelength region. The second group of samples (2) concerned samples with AR14. As in the scores plot obtained for PCA1 (Fig. 17), the presence of AR14 was also linked with PC1. In fact, samples with increasing dye concentration were distributed along the PC1 axis in the positive direction. The third group of samples (3) concerned Ag-NP suspensions in Emsize E1 and mineral solutions and it is visible that Emsize E1 was not significantly described by PC1 or PC2 and that changes in the mineral content could be described by PC2, with score values decreasing with its increase.

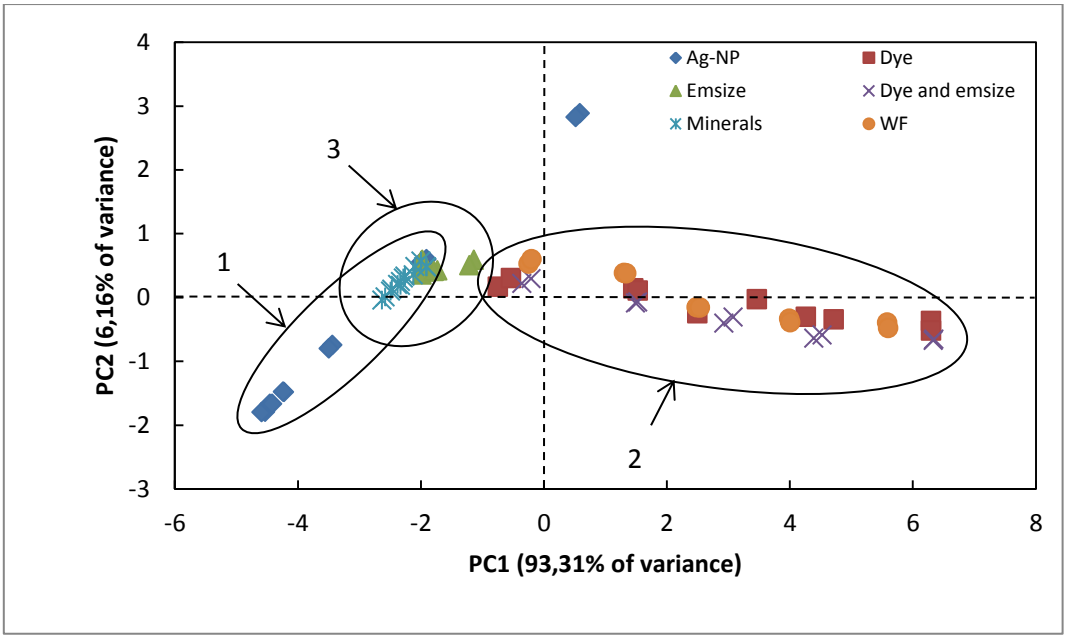

Figure 23 – Scores plot of PC1 and PC2 from PCA4 model.

In the PCA3 model, PC1 and PC2 captured 96.44% and 3.17% of the total variance present in the dataset, respectively. In the PCA4 model, 93.31% and 6.16% of the variance was captured by PC1 and PC2, respectively.

The Q residuals against Hotelling's T^2 for PCA3 are represented in Fig. 24. It can be seen that all the samples had a relatively similar behavior, apart from the previously mentioned samples corresponding to Ag-NP suspensions in 50 mg L^{-1} dye solution and samples of Ag-NP suspensions containing 2, 5 and 100 mg L^{-1}. Similarly to PCA1, samples corresponding to Ag-NPs suspended in 5 g L^{-1} Emsize E1 solution were not well described by the PCA3 model. Additionally, samples of Ag-NPs suspensions in dye and Emsize E1 solutions with a dye concentration 50 mg L^{-1} were also not well described by the PCA3 model, as is shown in the Fig. 24. The Q residual limit for PCA3 was 0.39% (Fig. 24).

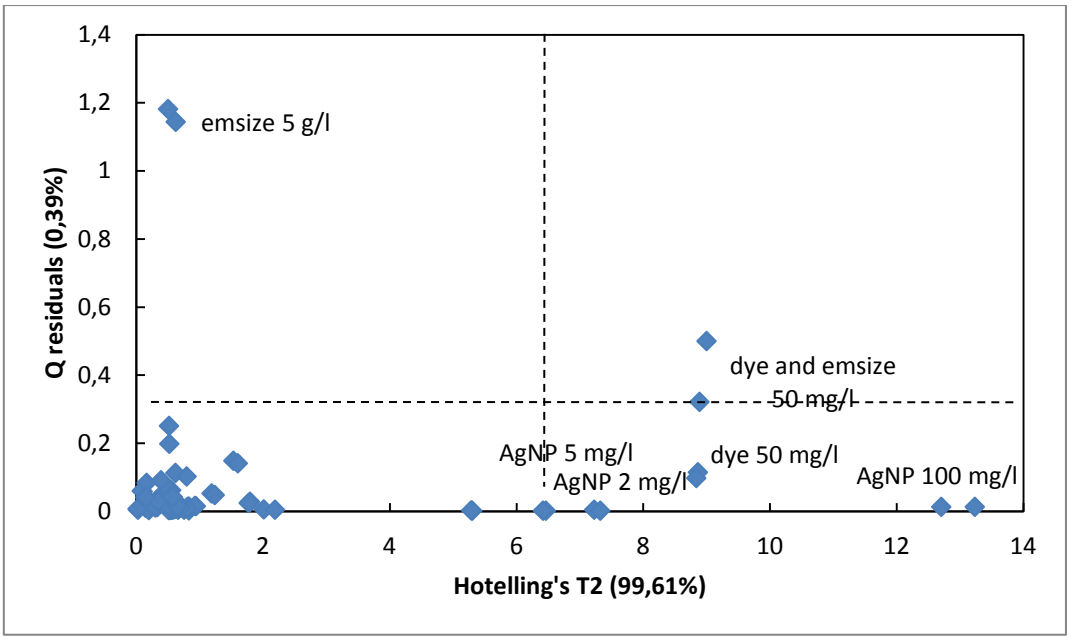

Figure 24 –Hotelling's T^2 and Q residuals for PCA3 model

The Q residuals against Hotelling's T^2 plot for PCA4 are presented in Fig. 25 and the results were similar to the ones described for PCA3 with a Q residual limit of 0.53% (Fig. 24). However, for PCA3, most of the samples lay in the Hotelling's T^2 range of 0-2. After excluding the samples containing 50 mg L^{-1} AR14 in PCA4 (Fig. 25) this range increased to 0-5%.

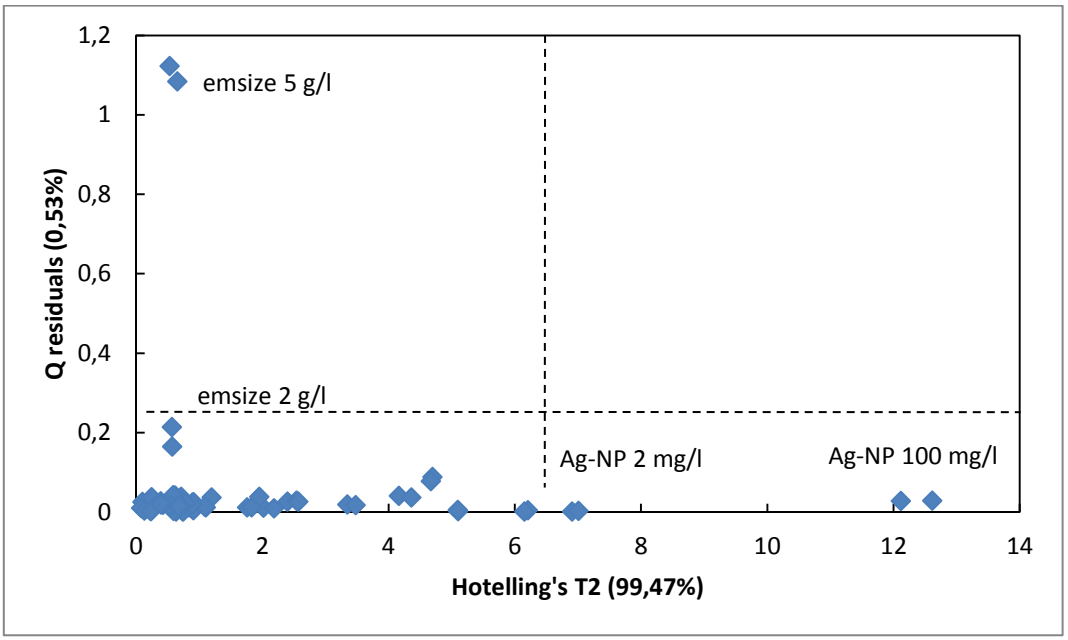

Figure 25 – Hotelling's T^2 and Q residuals for PCA4 model

4.2.2.3 PCA5 and PCA6 model interpretation – vector loadings, scores plot and Q residuals

PCA5 and PCA6 models were developed using the shorter wavelength range of 250-400 nm corresponding to the UV-Vis signal of Ag-NPs in water. In Fig. 26 it is seen the one-vector loading plot of PC2 of PCA5, which contains information regarding Ag-NP concentration. The fragment of a normalized UV-Vis spectrum of a 50 mg L^{-1} Ag-NP suspension in water is also shown for comparison. As it is seen, PC2 describes the absorbance phenomenon around 317 nm related to Ag-NP content in the samples. Similar results were also obtained for the PCA6 model (not shown).

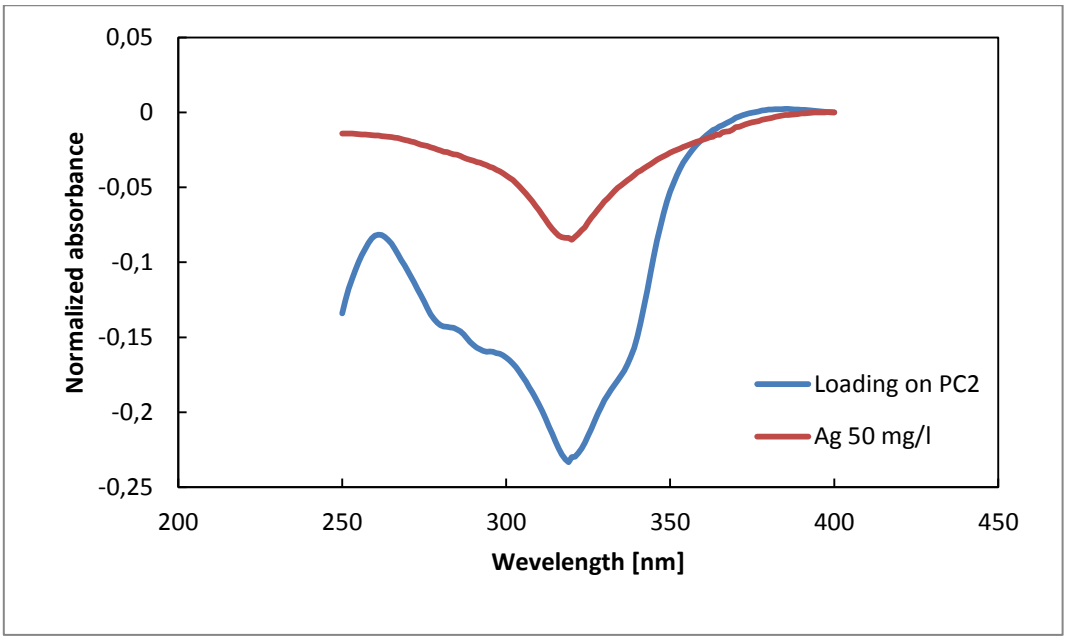

Figure 26 – One-vector loading of PC2 for PCA5 in comparison with a normalized spectrum of a 50 mg L^{-1} Ag-NP suspension in distilled water in the 250-400 nm wavelength range.

In Fig. 27, the scores plot for PC1 and PC2 of PCA6 model is presented, including the UV-Vis spectra in the 250-400 nm wavelength range and excluding the samples with 50 mg L^{-1} AR14 concentration, since they presented a behavior significantly different than the others. This plot was selected instead of the one corresponding to PCA5 (with the samples containing 50 mg L^{-1} AR14), due to a better visualization of the relationships between the samples. As it is seen in Fig. 27, four different groups of samples were identified. The first group (1) describes the samples of Ag-NP suspensions in water. Samples with increasing Ag-NP concentration were distributed along the PC2 axis in the positive direction. In this PCA model, PC2 had a relevant distinguishing effect for group 1, similarly to PCA4 (Fig. 23). The second group (2) was composed of samples containing different concentrations of dye and was regularly distributed along the PC1 axis, while the scores on PC1 approached the values corresponding to the 50 mg L^{-1} Ag-NP suspension in water. The third group (3) included samples with different concentration of minerals. As it is seen, the scores on PC1 did not change significantly for

this group of samples, but there differences along the PC2 axis were observed, with scores on PC2 decreasing with the increase in mineral concentration. The last group (4) consisted of samples with different concentrations of Emsize E1. The distribution of this group of samples is apparently independent of PC2, whose values remained constant and similar to the ones corresponding to the 50 mg L^{-1} Ag-NP suspension in water.

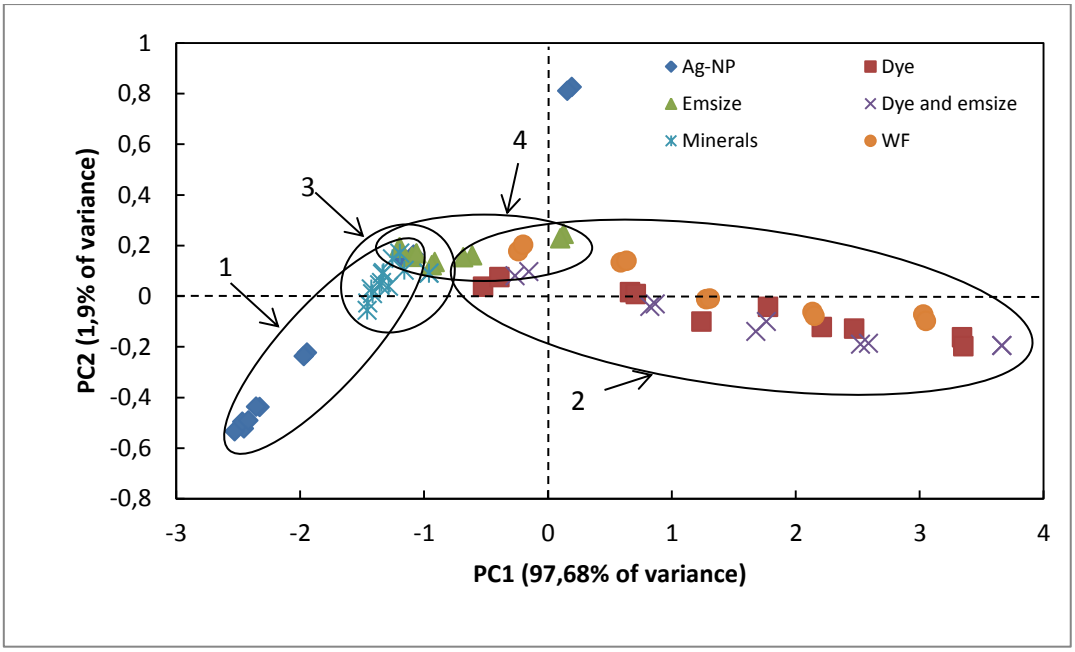

Figure 27 – Scores plot of PC1 and PC2 from PCA6 model.

In the PCA6 model, PC1 and PC2 are represented 97.68% and 1.9% of the total variance of the data set, respectively, while in PCA5, PC1 and PC2 represented 98.84% and 0.9%, respectively. Thus, these two PCs featured 99.74% of variance for PCA5 and 99.58% of variance for PCA6.

In Fig. 28 it is shown the plot with Hotelling's T^2 and Q residuals for PCA5. Similarly to the previous models, it can be seen that most of the samples are well described by the model. Samples with 50 mg L^{-1} dye concentration and with 2, 5 and 100 mg L^{-1} Ag-NPs concentration can be considered different from the others. The sample with 5 g L^{-1} Emsize E1and the sample with 50 mg L^{-1} dye and Emsize E1 were not well described by the PCA model. For PCA5, Q residuals limit was 0.25% and for PCA4 it was 0.42% as is shown in Fig. 28 and Fig. 29, respectively.

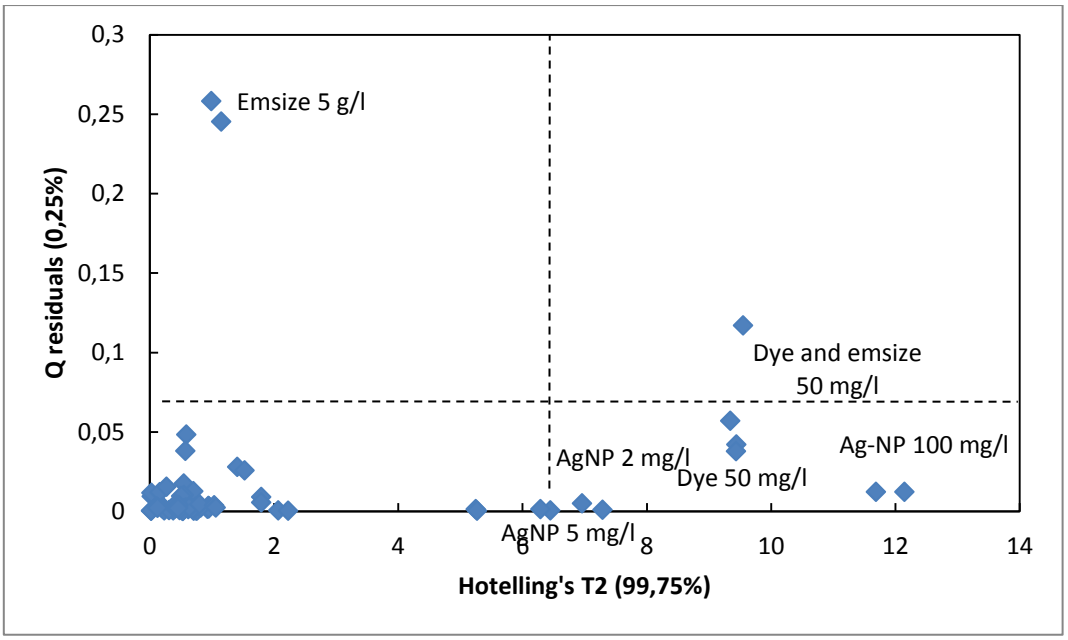

Figure 28 – Hotelling's T^2 and Q residuals for PCA5 model

In Fig. 29, it is shown the Q residuals against Hotelling's T^2 plot for PCA6 model, which was developed excluding the samples with dye concentration of 50 mg L^{-1}. As it is seen, the results are similar to the ones described for the previous PCA models. This plot is analogous to the one in Fig. 28 however samples are more distributed along the Hotelling's T^2 axis, evenly distributed in the 0-6 range. Another difference related to the sample with 2 g L^{-1} Emsize E1, which is on the border of the model.

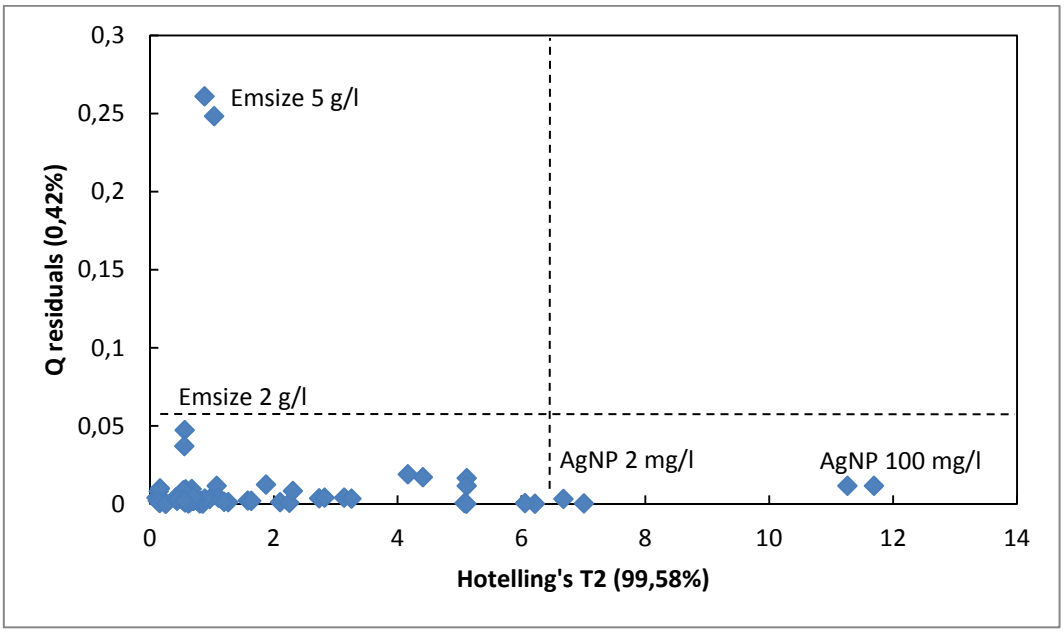

Figure 29 – Hotelling's T^2 and Q residuals for PCA6 model

4.3 PLS model development for the quantification of Ag-NPs in wastewater suspensions

The aim of this part of the work was the development of calibration models for the quantification of Ag-NPs in wastewater samples. These models were developed based on UV-Vis spectral data of samples corresponding to Ag-NP suspensions with different concentrations in water, presented in Fig. 30.

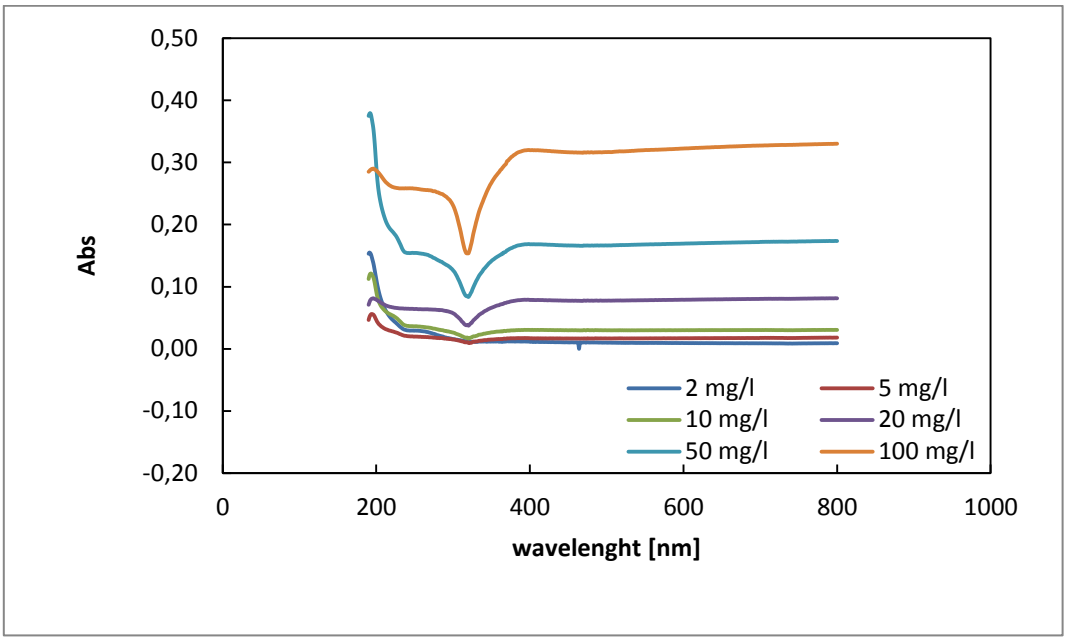

Figure 30 – UV-Vis spectra of samples with different Ag-NP concentrations in distilled water.

Due to the differences observed in the 400-800 nm spectral region, a spectral normalization procedure was tested, corresponding to normalization for the 700 nm wavelength. From each absorbance value of a spectrum it was deducted the absorbance value at 700 nm of that spectrum, which was almost the same value for all measured samples. The normalized spectra are presented in Fig. 31. Comparing the raw with the normalized spectra, it can be seen that this normalization does not enhance the differences between the spectra and for that reason the calibration models were developed using the raw spectra without normalization.

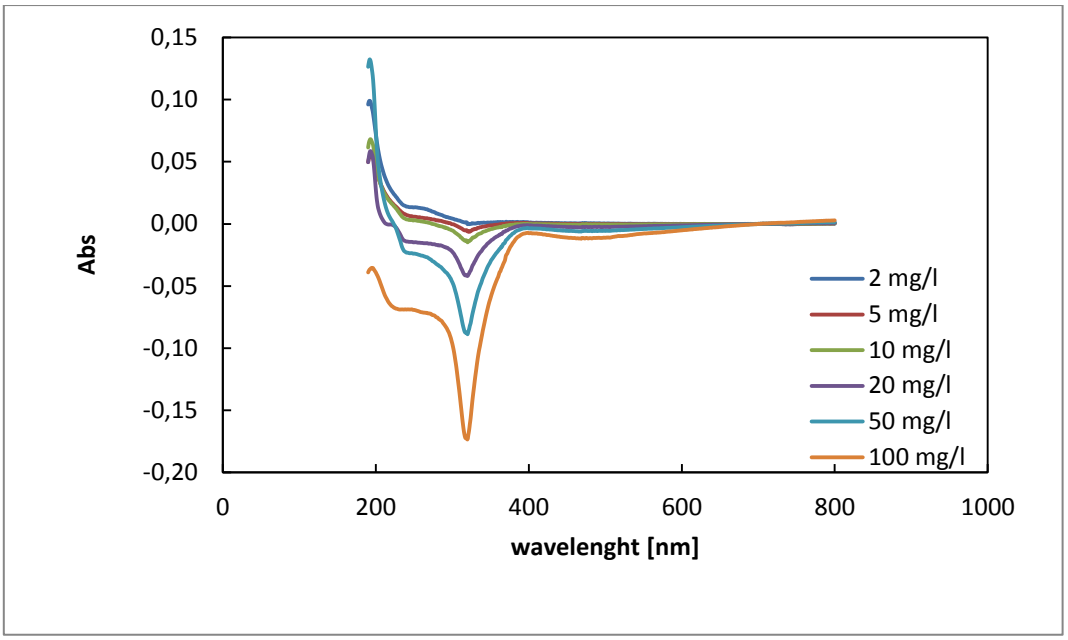

Figure 31 – UV-Vis spectra for samples with different Ag-NP concentration normalized for the absorbance measured at 700 nm.

A univariate calibration model was developed using the absorption values at the 317 nm wavelength, which corresponds to the typical absorption phenomenon of Ag-NPs in the UV-Vis spectral region. A multivariable PLS calibration model was also developed using the complete UV-Vis spectral data presented in Fig. 30. A comparison between these two models is presented in Fig. 32.

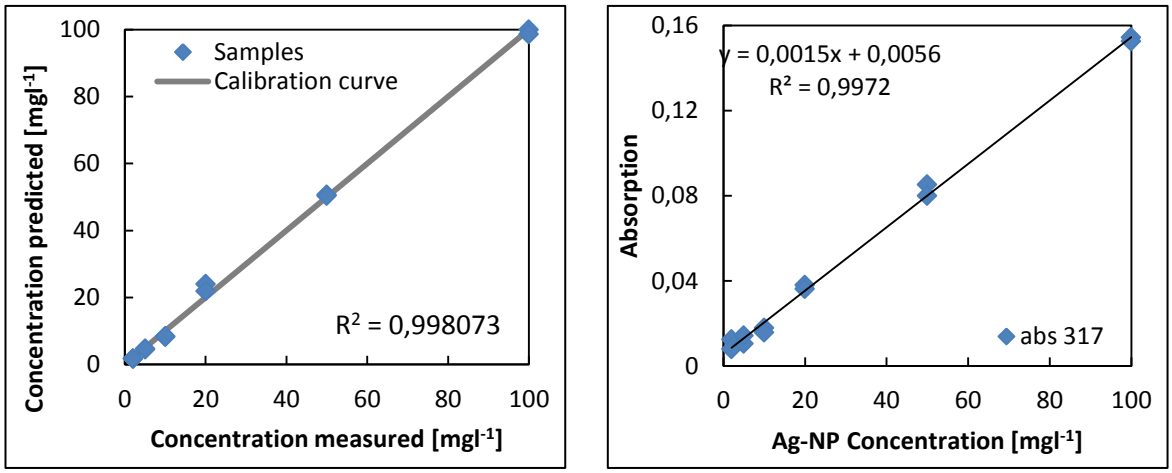

Figure 32 – Comparison between a multivariate PLS model calibration model (1) and a univariate calibration model (317 nm) for the estimation of Ag-NP concentration in wastewater (2).

Both the univariate and the multivariate models gave comparable results in terms of high value of the coefficient of determination (R^2). In fact, the PLS model presented an R^2 value of 0.998 and the

univariate model 0.997. There is a high agreement between the measured Ag-NP concentration values (X axis in Fig. 32 (1)) and model predicted values (Y axis in Fig. 32 (1)). However, a great advantage of the PLS model is the fact that it was developed directly from the raw data without any additional spectral pre-processing except for mean-centering and even though exhibited such accuracy. Additionally, the fact that this model was developed using the complete range of the UV-Vis spectra and not only one wavelength as in the univariate model (317 nm), confers it a higher flexibility for the prediction of Ag-NP concentration in suspensions with different matrix composition. For example, it may be useful for samples with Ag-NPs that have undergone aggregation, since the absorbance phenomenon in the visible region typical of Ag-NPs is dependent on particle size. Thus, it is expectable that a calibration model using the whole UV-Vis spectrum will have a better performance than a univariate model.

5. CONCLUSION

In the present work two main objectives were pursued. The first was the off-line monitoring and performance comparison of three SBRs inoculated with flocculent activated sludge and operated in order to promote the formation of aerobic granular sludge during the treatment of textile wastewater. The second was the development chemometric models based on UV-Vis spectroscopy for the qualification and quantification of Ag-NPs in wastewater suspensions.

Off-line monitoring of the three SBRs was carried out using COD analyses, measurements of TSS and VSS and UV-Vis spectroscopy of filtered samples.

COD analyses showed the performance of each bioreactor in terms of carbon substrate removal. In all three reactors, COD removal increased up to 45% after the adaptation period. This removal level was achieved mainly in the anaerobic reaction phase of the SBR cycle and it was almost unchanged during the subsequent aerobic phase. It can therefore be concluded that different feed flow regimes had no impact on COD removal.

Measurements of TSS and VSS served to assess the accumulation of biomass in the bioreactors. The biomass concentration increased from 3 to 8 gTSS L^{-1} and VSS/TSS varied within the 77-91% range in SBR1 and SBR2. SBR3 accumulated a lower concentration of biomass. It increased to less than 7 gTSS L^{-1} from an initial value of 3 gTSS L^{-1} and VSS/TSS values fluctuated between 78 and 88% along the reported granulation period. So it can be concluded that in SBR1 and SBR2, with a static feeding strategy, resulted in higher biomass accumulation than in SBR3 with a plug-flow feeding strategy.

Measurements of the residual dye concentration in the reactors were carried out using UV-Vis spectroscopy. The biomass adapted rapidly to the synthetic textile wastewater containing the azo dye AR14. Although the first monitored cycle showed a higher residual dye concentration in SBR1 than in SBR2, in subsequent cycles the differences between the two were much less significant. The highest achieved dye removal level was 87.5%. Dye removal occurred almost exclusively in the anaerobic phase of the cycle, with no substantial changes during the aerobic phase. Lower color removal levels were observed in SBR3, which was probably due to the shorter mixed anaerobic reaction phase, which is important for dye removal. The highest dye removal level in SBR3 was found to be 64%. Thus it can be concluded that this type of reactor and its operation regime is not as effective for dye reduction as those of the first two reactors.

Principal component analysis (PCA) was carried out by using the mean-centered UV-Vis spectra of raw measured samples from the prepared Ag-NP containing aqueous media. Individual behaviors for each of the tested component were well distinguished and described in the method plots. It can be said that UV-Vis spectroscopy with PCA is a potentially very satisfactory method quality monitoring in wastewater containing Ag-NPs.

Principal least squares (PLS) was used for the development of a calibration model for the estimation of Ag-NPs concentration values in wastewater samples using the mean-centered UV-Vis spectra of Ag-NP water suspensions with different concentrations. Two main advantages of the developed PLS model were found. The first advantage was the simplicity of the procedure, since the model was

developed using only raw spectral data without pre-processing methods and it was very accurate, as demonstrated by the determination coefficient values. The second advantage was that a model was developed from the whole generated dataset, using the entire range of wavelengths and including mixtures of different components, thus reflecting more closely the complexity of real wastewater samples. It was thus more flexible than the alternative model developed using absorbance readings at only one wavelength. Furthermore, considering that the absorbance phenomenon in the visible region typical of Ag-NPs is dependent on nanoparticle size, a multivariate calibration model developed using the entire UV-Vis wavelength range is potentially more adequate to estimate the concentration of AG-NPs in wastewater in the presence of nanoparticle aggregation phenomena.

6. BIBLIOGRAPHY

Abdi, H., Williams, L. J., 2010. Principal component analysis. *Wiley Interdisciplinary Reviews: Computational Statistics*, 2, pp. 433-459.

Beebe, K. R., Kowalski, B. R., 1987. Comparison of multivariate calibration and analysis. *Analytical Chemistry*, 59, pp.1007 – 1017.

Choi, O., Deng, K. K., Kim, N.-J., Ross Jr., L., Surampalli, R. Y., Hu, Z., 2008. The inhibitory effects of silver nanoparticles, silver ions, and silver chloride colloids on microbial growth.*Water research*, 42, pp.3066-3074.

Clescerl, L. S., Greenberg, A. E., Eaton, A.D., 1999. *Standard Methods for Examination of Water and Wastewater* 20th ed., American Public Health Association.

deKreuk, M. K., Kishida, N., van Loosdrecht, M. C. M., 2007. Aerobic granular sludge - state of the art.*Water Science and Technology*, 55, pp.75-81.

dos Santos, A. B., Cervantes, F. J., van Lier, J. B., 2007. Review paper on current technologies for decolourisation of textile wastewaters: Perspectives for anaerobic biotechnology. *BioresourceTechnology*, 98, pp.2369-2385.

Eckschlager, K., 1991. Chemometrie. Praha: Karolinum, 156 s. ISBN 80-7066-487-8.

Haaland, D. M., Thomas, E. V., 1988a. Partial least-squares methods for spectral analyses. 1. Relation to other quantitative calibration methods and the extraction of qualitative information. *Analytical Chemistry*, 60, pp.1193 – 1202.

Haaland, D. M., Thomas, E. V., 1988b. Partial least-squares methods for spectral analyses. 2. Application to simulated and glass spectral data. *Analytical Chemistry*, 60, pp.1202 – 1208.

Isanta, E., Suárez-Ojeda, M. E., delRío, Á. V., Morales, N., Pérez, J., Carrera, J., 2012. Long term operation of a granular sequencing batch reactor at pilot scale treating a low-strength wastewater.*Chemical Engineering Journal*, 198-199, pp. 163-170.

Kittler, S., Greulich, C., Diendorf, J., Köller, M., Epple M., 2010.Toxicity of Silver Nanoparticles Increases during Storage Because of Slow Dissolution under Release of Silver Ions.*Chemistry of Materials*, 22, pp.4548-4554.

Li, A., Yang, S., Li, X., Gu, J., 2008. Microbial population dynamics during aerobic sludge granulation at different organic loading rates.*Water Research*, 42, pp. 3552-3560.

Lourenço, N. D., Chaves, C. L., Novais, J. M., Menezes, J. C., Pinheiro, H. M., Diniz, D., 2006. UV spectra analysis for water quality monitoring in a fuel park wastewater treatment plant.*Chemosphere*, 65, pp.786-791.

Lourenço, N. D., Lopes, J. A., Almeida C. F., Sarraguca, M. C., Pinheiro, H. M., 2012. Bioreactor monitoring with spectroscopy and chemometrics: a review. *Analytical and Bioanalytical Chemistry*, 404, pp.1211-1237.

Muda, K., Aris, A., Salim, M. R., Ibrahim, Z., Yahya, A., van Loosdrecht, M. C. M., Ahmad, A., Nawahwi, M. Z., 2010. Development of granular sludge for textile wastewater treatment.*Water Research*, 44, pp. 4341-4350.

Pronk, M., de Kreuk, M. K., de Bruin, B., Kamminga, P., Kleerebezem, R., van Loosdrecht, M. C. M., 2015. Full scale performance of the aerobic granular sludge process for sewage treatment.*Water Research*, 84, pp. 207-217.

Quan, X., Cen, Y., Lu, F., Gu, L., Ma, J., 2015. Response of aerobic granular sludge to the long-term presence to nanosilver in sequencing batch reactors: Reactor performance, sludge property, microbial activity and community. *Science of the Total Environment*, 506-507, pp.226-233.

Rocktäschel, T., Klarmann, C., Ochoa, J., Boisson, P., Sorensen, K., Horn, H., 2015.Influence of the granulation grade on the concentration of suspended solids in the effluent of a pilot scale sequencing batch reactor operated with aerobic granular sludge. *Separation and Purification Technology*, 142, pp.234-241.

Sheng, Z., Liu, Y., 2011. Effects of silver nanoparticles on wastewater biofilms.*Water research*, 45, pp.6039-6050.

van den Broeke, J., Langergraber, G., Weingartner, A., 2006. On-line and in-situ UV/vis spectroscopy for multi-parameter measurements: a brief review. *Spectroscopy Europe*, 18, pp. 15-18.

van der Zee, F. P., Villaverde S., 2005. Combined anaerobic-aerobic treatment of azo dyes-A short review of bioreactor studies.*Water Research*, 39, pp.1425-1440.

Venkatesan, P., Dharuman, C., Gunasekaran, S., 2011. A comparative study of principal component regression and partial least squares regression with application to FTIR diabetes data. *Indian Journal of Science and Technology*, 4, pp. 740 – 746.

Wan, J., Sperandio, M., 2009. Possible role of denitrification on aerobic granular sludge formation in sequencing batch reactor.*Chemosphere*, 75, pp.220-227.

Winkler, M-K. H., Kleerebezem, R., de Bruin, L. M. M., Verheijen, P. J. T., Abbas, B., Habermacher, J., van Loosdrecht, M. C. M., 2013. Microbial diversity differences within aerobic granular sludge and activated sludge flocks. *Applied Environmental Biotechnology*, 97, pp.7447-7458.

Wise, B. M., Gallagher N. B., 1996. The process chemometrics approach to process monitoring and fault detection. *Journal of process control*, 6, pp.329-348.

Wise, B. M., Gallagher N. B., Bro, R., Shaver, J. M., Windig, W., Koch, R. S., 2005. PLS_Toolbox 3.5 for use with MATLAB™. *Eigenvector Research, Inc.*, 830 Wapato Lake Road, Manson, WA 98831 USA.